UNIVERSITAT POLITÉCNICA DE VALÉNCIA

SCHOOL OF AGRICULTURAL ENGINEERING AND ENVIRONMENT

BACHELOR´S DEGREE IN BIOTECHNOLOGY

Cyanobacterial photosynthesis modelling for hydrogen production

Course 2015/2016

Author: Carlos Arévalo Villa

Thesis Director: Javier Urchueguía Schölzel

Experimental Director: David Fuente Herráiz

Valencia, september of 2016

Cyanobacterial photosynthesis modelling for hydrogen production

Summary

The problematic of the current dependence of fossil fuels and other non-renewable sources of energy, and how many biotechnological approaches, such as the production of biohydrogen in cyanobacteria, can help us to overcome this situation were discussed in this report. Here, the potential of *Synechocystis* sp. PC 6803 as a hydrogen biofactory was reviewed.

With that aim, a computational model developed using MATLAB as numerical computing environment was built from the ground. The objective of the model was to simulate the metabolical fluxes of electrons in the electron transport chain in the thylakoid membrane of *Synechocystis* sp. PC 6803, with particular emphasis on biohydrogen synthesis by the reversible oxygen-intolerant reversible [Ni-Fe] hydrogenase Hox.

While still in an early stage of development, this computational model has proved its capability to simulate the behavior of the photosynthetic electron transport chain of Synechocystis sp. PCC 6803 and the synthesis of biohydrogen under different conditions and modifications.

The future iterations of the model will be able to simulate additional mechanisms, while providing more accurate and biologically significant data to metabolic engineers.

Key words: Cyanobacteria, Synechocystis sp. PCC 6803, biohydrogen, Hox hydrogenase, Systems Biology and Metabolic Engineering, photosynthetic electron transport chain, computational model.

Author: Arévalo Villa, Carlos

Thesis Director: Urchueguía Schölzel, Javier Fermín.

Experimental Director: Fuente Herráiz, David

Valencia, september of 2016

Modelización matemática de la fotosíntesis en cianobacterias para la producción de hidrógeno

Resumen.

La actual problemática sobre la actual dependencia de los combustibles fósiles y otras fuentes no renovables de energía; y como diversos acercamientos biotecnológicos, tales como la producción de biohidrógeno en cianobacterias, pueden ayudarnos a superar esta situación, son discutidos en esta memoria. Concretamente, se analizó el potencial de Synechocystis sp. PC 6803 como posible biofactoría de hidrógeno.

Con dicho objetivo en mente, se desarrolló desde cero un modelo computacional usando MATLAB como entorno de programación. La intención de este modelo es simular los flujos metabólicos presentes en la cadena de transporte de electrones fotosintética de la membrana del tilacoide de Synechocystis sp. PCC 6803, con particular énfasis en la síntesis de biohidrógeno por la [Ni-Fe] hidrogenasa reversible intolerante al oxígeno Hox.

Aún en un temprano estado de desarrollo, este modelo computacional ha probado su capacidad para simular el comportamiento de de la cadena de transporte de electrones fotosintética de Synechocystis sp.PCC 6803 bajo diferentes condiciones y modificaciones.

Futuras versiones del modelo serán capaces de simular mecanismos adicionales, proporcionando resultados más precisos y biológicamente significativos a los ingenieros metabólicos.

***Palabras clave**: Cianobacterias, Synechocystis sp. PCC 6803, biohidrógeno, hidrogenasa Hox, Biología de Sistemas e Ingeniería Metabólica, cadena de transporte de electrones fotosintética, modelo computacional.*

Autor: Arévalo Villa, Carlos

Tutor Académico: Urchueguía Schölzel, Javier Fermín

Tutor experimental: Fuente Herráiz, David

Valencia, septiembre de 2016

Special thanks to:

Those whom I can call my family, for supporting me in the worst moments

My friends, for providing me with good advices and better moments

Those who dwell in their own darkness; there is always light at the end of the path

And finally, I want to dedicate this report to myself

Because me lo merezco.

Index

I. Introduction……..1

i. Current state of fuel and energy production……..1
ii. The hydrogen as an alternative……..4
iii. Hydrogen production pathways. Photobiological hydrogen production……5
iv. Objectives of the Degree Thesis.....7

II. Systems biology and metabolic engineering……..8

III. Synechocystis sp. PCC 6803 as H2 biofactory……11

i. The Electron Transport Chain……..12
ii. Non-linear ETC components: Cyclic transport, oxygen evolution and electron valves. ……22
iii. ATP-synthase: components of the protonmotive force……..24
iv. The bidirectional Ni-Fe hydrogenase……..26

IV. Applied Systems Biology: A model for the Synechocystis sp. PCC 6803 electron transport chain……..27

i. Reactions rate equations used in the model……28
ii. Molecules and reactions in the model……30
iii. Testing the model: robustness and possibilities……35
iv. Next steps in the development of the model……39

V. Conclusion……40

VI. References

Supplementary Files I and II

1. Introduction

1.1 Current state of fuels and energy production

Since the rise of the Industrial Revolution, the world has developed a strong dependence of fossil fuels to sustain the new kind of society that was born in that time. This dependence has grown in a pretty solid pattern during the last century, due to the increasing demand of energy the world has experimented, caused by the highly energy-dependent lifestyle of the occidental society, and more and more countries that were eminently rural-based 50 years ago, which in the last decades have transitioned to an industrialized model, such as China or India.

The growth of worldwide energy consumption has grown in a median of 1.9% during the last 10 years, being the increment in 2015 a 1.0% (BP P.L.C 2016). Despite the appearance of new renewable sources of energy (14% of global energy consumption in 2015) such as renewables (2.8%), hydroelectricity (6.8%) or even nuclear energy (4.4%), fossil fuels still represent the main source of energy production, representing an 85.9% of global energy consumption (32.9% oil, 29.2% coal, 23.8% natural gas).

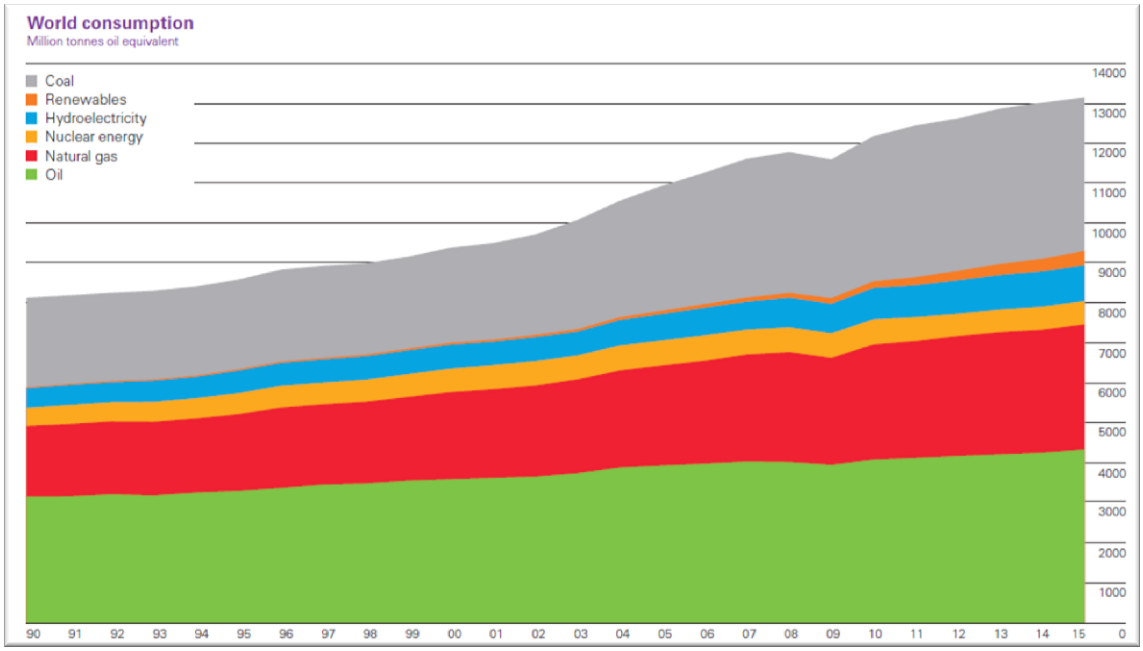

***Figure 1**. World primary energy consumption sorted by type of fuel, from 1990 to 2015.*

This tendency is even more accused in regions such as the Middle East (98% of fossil fuels) or Asia Pacific (51% of energy consumption comes from coal). Only in Europe/Eurasia non fossil sources reach more than a third of total energy consumption.

However, there´s been an increment of non-fossil sources of energy consumption: 1.3% in nuclear energy, 1% of hydroelectricity and 15.2% in renewable sources; coupled with a 1.8% decline of coal consumption (oil and natural gas have increased in 1.9% and 1.7% respectively). Despite of this positive pattern, CO2 emissions have not decreased, but even slightly increased 0.1% in 2015.

This situation leads to two important problems: first one, almost a half of the oil and natural gas reserves belong to political unstable regions, such as the Middle East: for oil, 47,3% of proved reserves are placed in Middle East; for natural gas, this proportion is 42.8% (Fig. 2A). This instability leads tremendous variations of the price of the crude oil barrel (Fig. 2B). Notice the price rises each time a remarkable event takes place in that region, reaching its historical maximum during the development of the so called "Arab Spring" (almost 120 US$).

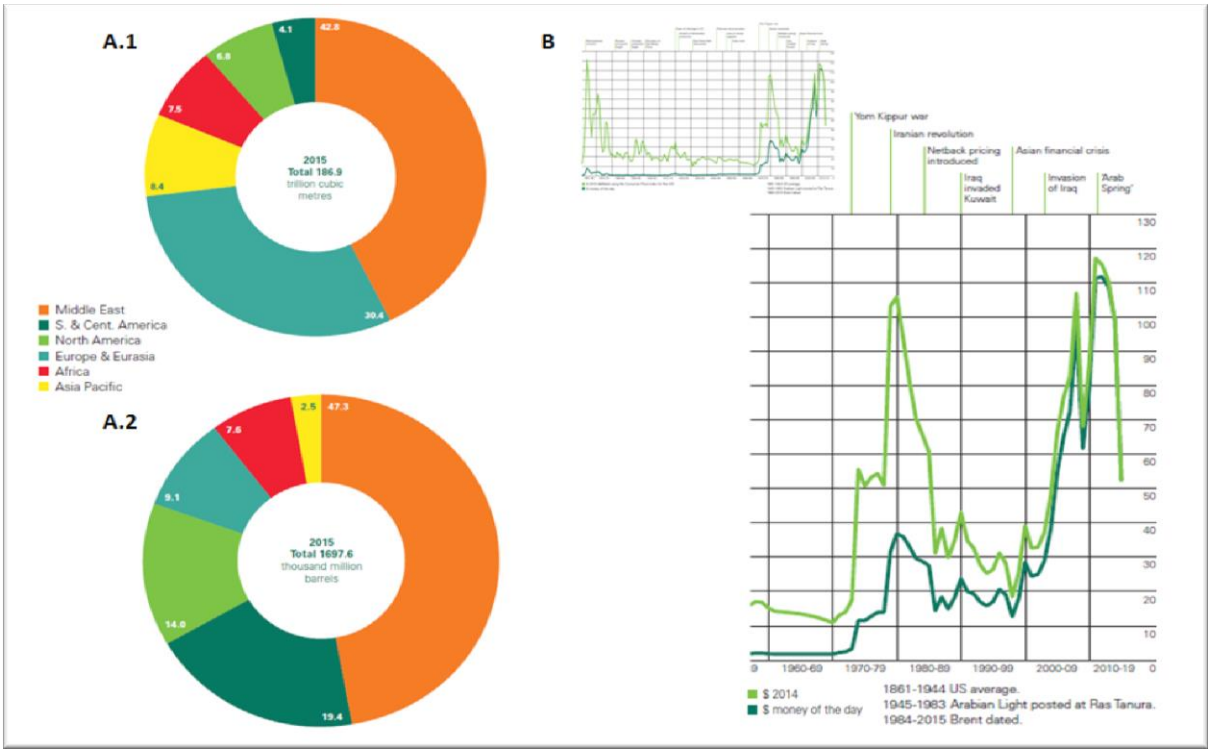

***Figure. 2**. (A) Distribution of proved reserves in 2015 of natural gas (A.1) and oil (A.2). (B) Crude oil barrel price variation from late 50´s to 2015.*

The other major problem is that, despite the increase of the use of clean sources of energy, the effort is still insufficient to reverse the escalation of CO2 emissions and therefore, the effects of climate change. From 1880 to 2012, the global temperature has increased a median of 0.85°C, being the last three decades the warmest in the last 1400 years (Fig. 3A) (IPCC, 2014). Over 90% of this energy increase has been stored in ocean warming, and only 1% has been stored in the atmosphere. This increase of temperature has resulted in a decline of the Artic sea-ice extent of 3.5-4.1% per decade (Fig. 3C); consequently, the sea level has augmented 0.19 m in the same period (Fig 3D). Additionally, the oceanic CO2 uptake has led to a 26% increase in acidity of oceanic waters.

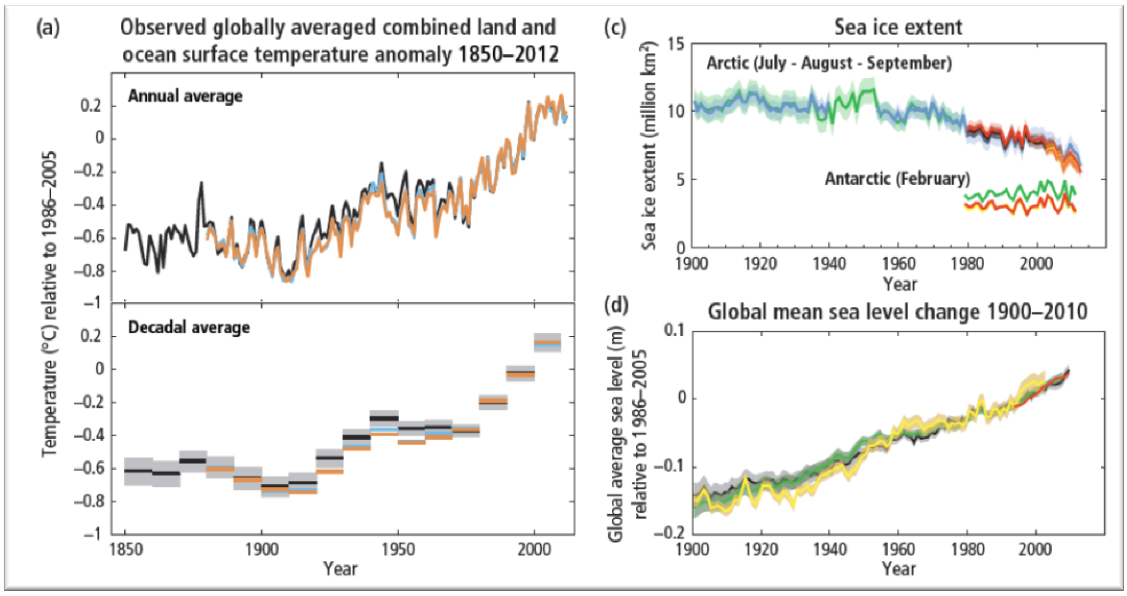

Figure 3. *A. Observed globally averaged combined land an ocean surface temperature anomaly 1850-2012. C. Sea ice extent 1900-2012. D. Global mean sea level change (1900-2010)*

The augment of all these parameters comes coupled with a spectacular increase of anthropogenic greenhouse gases emission. Over 2040 Gt of CO2 have been added to the atmosphere by human activity between 1750 and 2011, half of them during the last 40 years (Fig. 4). 40% percent of these emissions still remain in the atmosphere, while the rest has been absorbed by sinks like ocean, vegetation and soil. Most of the CO2 emissions come from combustion of fossil fuels, cement production and flaring.

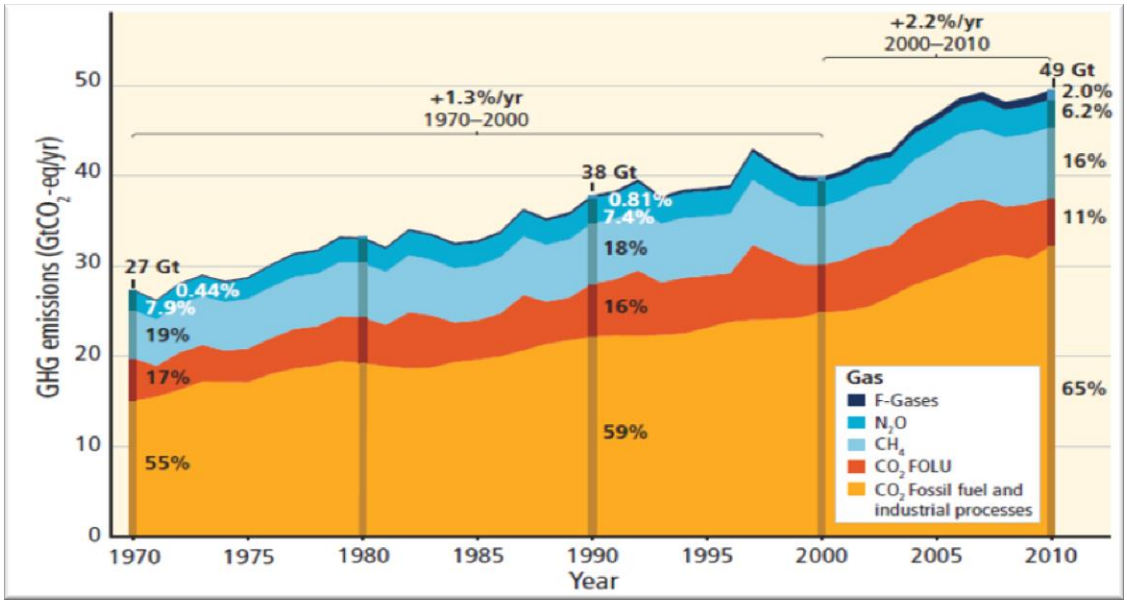

Figure 4. *Total annual anthropogenic GHG emissions by gases, from 1970 to 2010.*

The political strategy against GHG emissions and their impact to the climate change was discussed during the Paris Climate Change Conference 2015 (UN Treaty Collection, 2016). In the Paris Agreement from this conference, the main compromise between the parts, as

stated in Art.2 of this Agreement, was the compromise to maintain the rise of global temperature below 2°C, and to make further efforts to keep this augment under 1.5°C;by promoting a low GHG emissions development. But, during 2015, 33508.4 million tons of CO2 were emitted to the atmosphere, a 0.1% more than in 2014, and a 17% more than in 2005 (28533 million tons of CO2). It remains clear that, to reach the objectives acquired in the Paris Conference, it is necessary to find cleaner alternatives in the way the developed world produces its energy.

1.2 The hydrogen as an alternative

Amongst all the present alternatives to fossil fuels, the hydrogen stands out as one of the most promising. As an energy vector, hydrogen presents many benefits:

- Hydrogen is the most abundant element on the universe. Since molecular hydrogen as a gas doesn´t occurs naturally on Earth, it is present in many other forms, from water through biomolecules like carbohydrates, so it can be produced from a great range of substrates.
- Hydrogen is the highest energy dense fuel known, with a Low Heating Value (LHV) of 120.07 MJ/Kg, while the same value for gasoline and natural gas are 43.44 and 48.63 MJ/Kg respectively, around a third of the energy potential of the hydrogen.
- Combustion of hydrogen produces zero CO2 emissions, producing only water as byproduct. By contrast, the employment of fuels from biomass not only do not reduce the CO2 emissions, but increase them because of the so called "carbon debt", which is "*the amount of CO2 released during the first 50 since the land conversion from natural habitat to cropland due to burning or microbial decomposition of organic carbon stored in biomass and soil*" (Fargione et al, 2008).
- Hydrogen as an energy vector is very safe for transport, storage and use.

This does not mean that the employment of hydrogen suppose a flawless alternative to fossil fuels. The development of a "hydrogen economy" stands against many drawbacks and challenges:

- Storage. Liquidification of hydrogen for its transport and use as a fuel requires high-pressure, low temperature conservation, which requires a high amount of energy, lowering its great energy efficiency.
- Lack of infrastructure. Nowadays, there´s no enough infrastructure available to allow the normal population to use hydrogen in an easy and cheap way.
- Flammability. Hydrogen is extremely flammable, which makes necessary a special treatment and additional safety measures.

1.3 Hydrogen production pathways. Photobiological hydrogen production.

As stated before, there are many ways to produce hydrogen from many different sources, but we are only focusing on those called "Green Hydrogen Pathways" (Fig. 5) (FCH JU, 2015), being "green hydrogen" the hydrogen produced using only from only renewable sources.

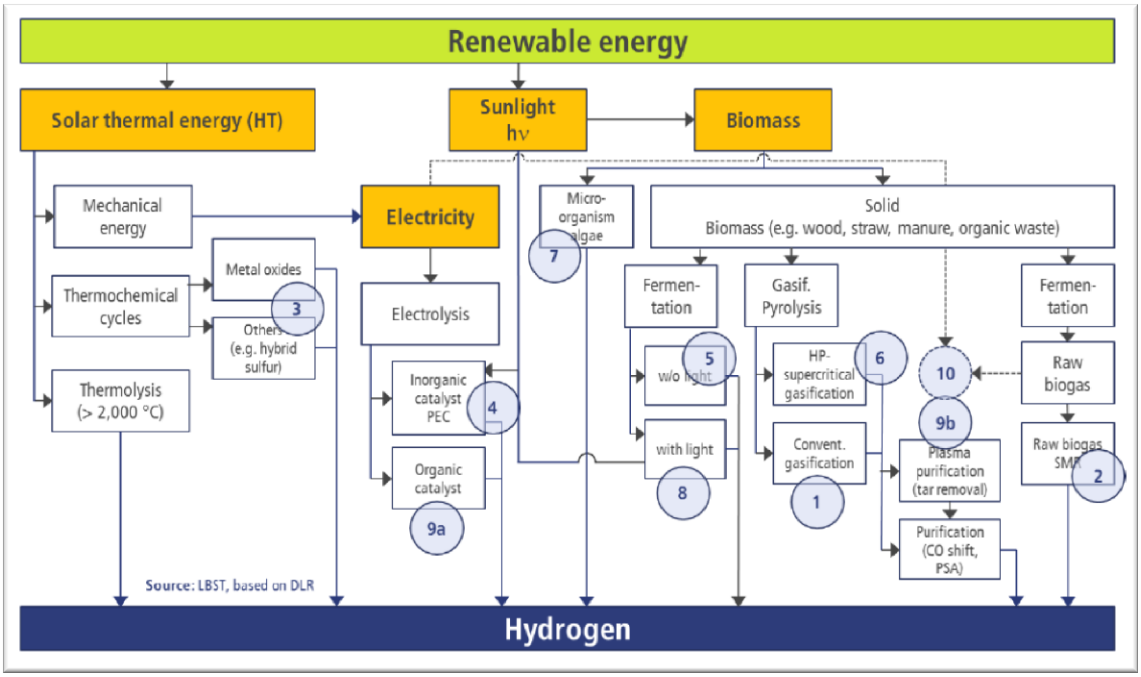

***Figure 5**. "Green hydrogen" production pathways.*

The most representative pathways are:

- **Biomass pyrolysis and gasification**. This method consists of the pyrolysis of lignocellulosic biomass, giving methanol and other primary gases; followed by a direct (using O2 as gasification agent) or indirect (using water as gasification agent) gasification, giving CO, H2, CO2 and methane. The output of this process is hydrogen with 99.8% purity; ashes, used bed material and flue gas are the wastes of this process.
  Although this technology is well developed and close to its application in the real world, it still faces major challenges being consistent quality of biomass required for the stability of the process and gas quality, and feedstock availability.

- **Raw biogas reforming**. Hydrogen can be produced directly from the combustion of the methane from biogas in a Steam Methane Reformer (SMR). The yield of the process is a gas mixture with 64-74% of hydrogen content (depending of the CO2 proportion of the input gas), which can be lately purified to produce pure hydrogen.

This technology is completely mature at the date, but needs further development for production and maintenance cost reduction.

- **Thermochemical Water Splitting**. This pathway is based on the oxidation of a metal oxide, or an oxidable fluid by reacting with water, in a two-step process:

  1. Oxidation of metal oxide (MO) by water. This process takes place at low temperatures:
  $$MO + H20 \rightarrow H2 + MO2.$$
  2. Recycling of the MO by stripping one oxygen atom. This process takes place at high temperatures (1600-1800°C):
  $$MO2 \rightarrow MO + \frac{1}{2}O2$$

  This technique produces zero emissions, with only H2 and O2 as products, and the energy needed to generate the high temperatures can be obtained by clean ways like solar energy. However, the extreme temperatures required and highly corrosive environment produced lead to a rapid degradation and a short lifetime of the components of the reactor. This technique also compels the employment of rare and expensive materials like cerium. The necessity of high direct solar irradiation limits its usage to certain regions.

- **Photocatalysis**. This technology is based on the usage of photo-electrochemical cells (PEC), devices that combine both photovoltaic electricity generation and water electrolysis (Fig. 6). The PEC consists of an anode and a cathode separated by an electrolyte. When irradiated with sunlight, the electrons of the anode shift their valence to the conduction band, leaving holes in the valence band that are replaced by the decomposition of OH- radicals into O2 and water. The electrons from the conduction band move to the cathode, where water is split into H2 and OH- radicals, which move to the anode and restart the cycle.

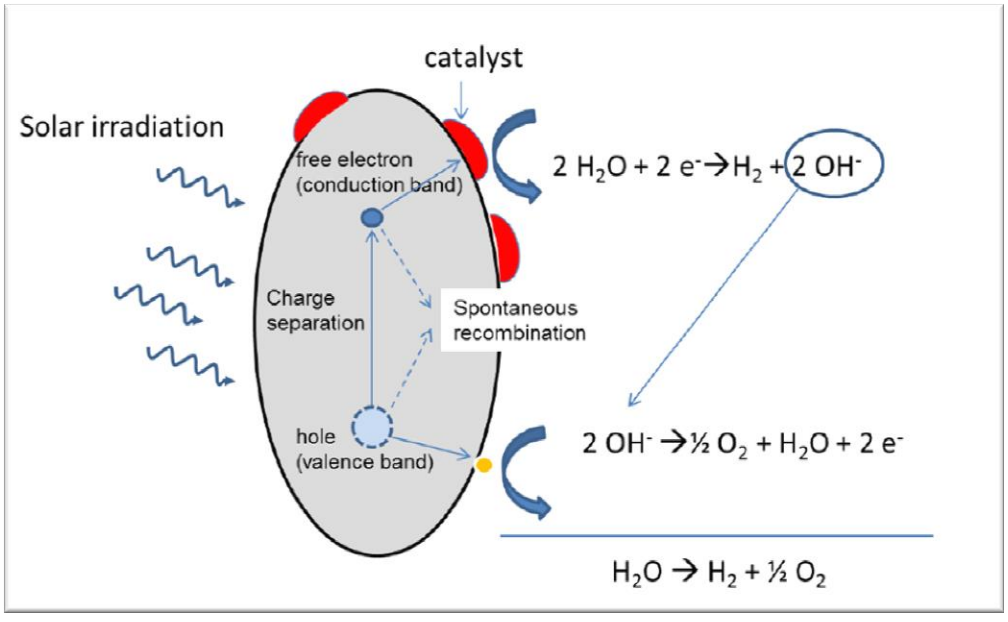

***Figure 6**. Functioning of the photocatalysis in a PEC.*

This main advantages of this technology are its high scalability, a low temperature process and a theoretical low price (5-6$/kg H2 expected in 2020). By contrast this technology requires large production areas and a further development to increase stability and lifetime of the PECs

- **Photo-biological Water Splitting.** Photosynthetic microorganisms such as microalgae and cyanobacteria are able to absorb sunlight to split water through photolysis using the known as "photosystems", protein complexes capable of gather solar energy and use it to split water and excite its electrons. These excited electrons enter the Electron Transport Chain (ETC), a chain of protein complexes used by the cell to generate redox power and ATP through the generation of a proton motive force (pmf), by the transport of the electrons from a high energy state to a low energy state.

  Apart from the production of ATP and NADPH, the ETC presents some other electron valves used by the ETC to deal with an excess of electrons, amongst we can highlight the so called "hydrogenases", enzymes capable to harvest this electron excess and transmit it to protons (H+), generating H2.

  This technology has the largest hydrogen production potential, though it only requires water and sunlight as inputs. Nevertheless, its energy conversion rate from solar energy to hydrogen is very low, around 1%; photobiological hydrogen production is fairly low developed, and it is the objective of many organizations and laboratories to overcome the current challenges it stands against.

As seen in the previous pages, hydrogen is one of the most promising energy sources of the future: its cleanness, availability and ease of production represent a good alternative to the traditional fossil fuels and many renewable sources like biofuels. Amongst the many ways to produce hydrogen in a big scale, photobiological hydrogen production stands as the most promising one, even though its development degree is still quite low.

The aim of this project is to provide new tools for the improvement of this technology, coming from the union between biology and engineering: synthetic biology and metabolic engineering.

1.4 Objectives of the Degree Thesis

During this Degree Thesis, the production of biohydrogen in Synechocystis sp. PCC6803, focusing specially in the photosynthetic electron transport chain of this cyanobacteria, will be reviewed.

Using this information, a computational model of this electron transport chain based on a system of ordinary differential equations (ODEs) will be created using the numerical computing environment MATLAB. This model will be used to simulate the behavior of the electron transport chain and specific trends of the metabolic fluxes related to it.

Specifically, the photoproduction of hydrogen by the oxygen-intolerant Ni-Fe reversible hydrogenase of Synechocystis will be simulated under various conditions, with the aim of maximizing the electron fluxes into this hydrogenase, and thus the synthesis of biohydrogen, while studying the inhibitive effect of oxygen produced during the photosynthesis process. Other components of the electron transport chain may be simulated and discussed.

As the hydrogen rises as one of the main alternative fuels in the future, and photoproduction of hydrogen by cyanobacteria suppose the most promising hydrogen production technology, the interest on improving the synthetic capabilities of cyanobacteria by the employment of metabolic engineering techniques is one of the maximum significance. The model here described will suppose a powerful tool for these metabolic engineers, since it will allow testing many genetic modifications *in silico*, therefore allowing them developing their investigations in a quicker, more efficient fashion.

2. Systems biology and metabolic engineering

Cells as a whole are not just the addition of many simple elements, but complex systems which functioning is based both on individual elements and all the specific interactions produced between them. Traditional biology has been focused on understanding these individual elements, and decipher, one by one, the specific interactions between elements; despite thanks to this work many advances have been made, if we want to use living organisms as molecular factories, this approach is totally insufficient; since cell machinery doesn´t work as a sum of individualities, we need to apply a new holistic approach that help us understand the organism as a global system: the systems biology.

The systems biology main characteristic relies on a deviation from the traditional procedure: instead of focusing of understanding the characteristics of the different molecules of the cell, the systems biology tries to find out the whole system structure and dynamics. This can be resumed in four answers to be solved (Kitano,2002a):

- **System structure**. The first step is to construct the full image of all the biochemical pathways involved, and how this pathways influence the physical and chemical properties of the singular cell or multicellular organisms.
- **System dynamics**. Next thing to ascertain is how the system behaves over time under many different conditions. This can be understood using metabolic analysis, or by identifying concrete mechanisms activating only under specific conditions.
- **Control method**. Understanding the mechanisms that control and regulate the state of the cell is the key to understand and minimize possible malfunctions of the system, and even provide a wide range of new elements to control the final output of the system.
- **Design method**. Once the previous questions are answered, it is necessary to develop a strategy to build up a biological system which the desired behavior. The way to integrate all the knowledge previously acquired, while developing a tool

that can far- reaching enhance and empower the design process, is to create computational models of the metabolic network, whose simulations can quickly give us the answers that otherwise would take many experiments and much more time to provide the feedback needed to improve our biological construct.

Therefore, systems biology introduces a new concept in biotechnological research typical from engineering: the employment of computational simulations to drive the direction of the development of new biotechnological tools (Fig. 7). The computational biology is based on two pillars: knowledge discovery and simulation based analysis (Kitano,2002b). Despite many tools are available to construct mathematical models, it´s not been since the latest advances in molecular biology are finally able to provide with the biological data required to support simulation-based researches.

Still out of the focus of the mainstream scientific research, computational modelling related to systems biology is becoming a powerful tool which role is going to be vital in the latest revolution of biotechnology: the metabolic engineering.

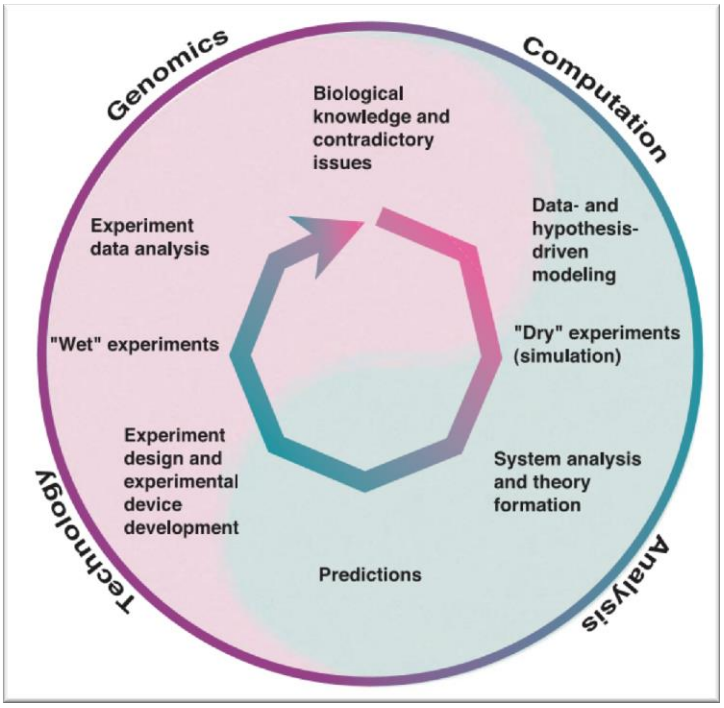

Figure 7. *Workflow cycle of a simulation based research in systems biology. Departing from biological knowledge given by "wet" experiments, a model can be constructed to execute "dry" experiments (in silico), whose results can be used both to design new biotechnological tools or to drive new experiments whose results start another iteration of the cycle.*

The metabolic engineering is defined as "*the directed improvement of cellular properties through the modification of specific biochemical reactions or introduction of new ones, with the use of recombinant DNA technology*"(Stephanopoulos, 1999). This means the capability not only to improve the efficiency of the production of biological compounds in loving organisms, but also the ability to produce whole new molecules and materials coming from low-efficiency, difficult management organisms, in well-known and more manageable organisms like E.coli or cyanobacterias. The latest advances on DNA editing

technologies, like the CRISPR/Cas system (Ann Ran, 2013), have made possible impressive applications, from pharmaceuticals and fuels to metamaterials like the spider silk. Though many new and different applications are to come into this discipline, the trade-offs of using living organisms as biofactories are common for all of them (Keasling, 2010):

- Cost and availability of starting materials.
- Metabolic routes and corresponding enzyme-coding genes identification.
- Designation of the most appropriate microbial host.
- Genetic control system for the desired metabolic pathways and the chosen host.
- **Methods for debugging and debottlenecking the constructed pathway.**
- **Ways to maximize yields and productivity**.

Molecular biology can easily solve the four first of these trade-offs, but for the latest two, systems biology represent a great advance.

In engineering, the employment of models and simulations that allow the researcher predict and decide which components are better to add to his design, and how these components are going to behave into the whole system is a common practice. This is not the case in the development of new biotechnological products, where the development state of modelling tools is still in its infancy, due to the absence of high-throughput genomic and metabolic data; but the latest advances in genomics, proteomics and metabolomics, coupled with the improvement of specific software and computational power are solving this problematic, and slowly but robustly the number of research teams that are joining the train of systems biology is increasing.

For the expansion of this knowledge and the proper evolution of this discipline, it is crucial that researchers along the globe have the capacity to share their models with other teams. As important as having a way of exchange, it is essential to create standardized modelling tools that allow the researchers to use parts of models developed by other teams in the creation of their own system. The main repositories pushing in that direction are:

- **Systems Biology Markup Language** (SMBL; http://www.sbml.org/). SBML describes itself as a "machine readable format for representing models, oriented towards describing systems where biological entities are involved in, and modified by, processes that occur over time". Beginning in 2003, the goal of the SBML development team is to serve as a declarative representation language for computational models in biology, while producing standards for the modelling community in an open, systematic and transparent fashion. The latest iteration of SBML, known as SBML 3, introduces the modular approach, where researchers have a defined core set of features and optional packages adding features on top of that core.

- **CellML** (http://www.cellml.org/). Developed vby the Bioengineering Institute at the University of Auckland, the CellML language is an open standard based on the XML markup language. CellML allows researchers to share models with other researcher, even if the teams are using different model-building software. CellMl includes information about model structure, mathematics and metadata. The

future goal of the CellML team is to be able to use other existing languages to specify data, define simulations and rendering information.

In conclusion, the development of new biotechnological tools based on the knowledge coming from the engineering world opens a broad range of future possibilities in the field of using organisms as machine to produce desired biomolecules.

3. Synechocystis sp. PCC 6803 as H2 biofactory

Synechocystis sp. PCC 6803 is an unicellular non-nitrogen fixing cyanobacterium, and the very first phototrophic organism whose genome was fully sequenced (Kaneko et al, 1996), being also the fourth genome-sequenced organism. Synechocystis sp. PCC6803 is one of the most popular organisms for genetic, physiological and bioengineering studies due to two main factors:

- It is naturally transformable by exogenous DNA (Grigorieva and Shestakov, 1982). This makes silencing or adding genes or even whole metabolic routes from other organisms quite easy, and so providing a powerful tool for metabolic engineers.
- Grows heterotrophically at the expense of glucose (Ripka et al., 1979; Williams, 1998). This makes possible to gather a wide broad of metabolic routes into an only organism, both light-driven or not.

Synechocystis is an unicellular coccoid lacking vesicles or a sheath. From the 3167 genes, 128 are involved in the various stages of the photosynthesis, and 224 are significantly homologous to the genes of higher plant plastids, including those related to PSI and PSII, the electron transfer chain, CO2 fixation, etc. (Ikeuchi and Tamato, 2001).

Synechocystis sp. PCC 6803 has several characteristic that made it very suitable for the production of alternative fuels (Quintana et al., 2011):

- Can contain a high quantity of lipids in its thylakoid membrane
- Its photosynthetic rate is higher than the one from algae or higher plants
- It requires low basic nutritional requirements: N2 and CO2 from the air, mineral salts, water and light as energy source.
- Cultivation is simple and cheap

Due to its high genetic malleability and metabolic characteristics, Synechocystis has been used to produce a wide range of fuels: ethanol (Dexter and Fu, 2009), photanol (Hellingwerf and de Mattos, 2009), biodiesel (Rittman, 2008), etc.

Synechocystis sp. PCC 6803 can produce hydrogen from two ways, both coupled to the Electron Transport Chain(Hall et al., 1995): as a byproduct of a nitrogenase under nitrogen limiting conditions (Gutthan et al, 2006) or by the Ni-Fe reversible hydrogenase, a hydrogenase capable of consuming or producing hydrogen depending on the redox state

of the cell (McIntosh et al., 2011). This hydrogenase is also highly intolerant to O2 produced in photosynthesis, and the competition with other major reducing agents like ferredoxin or NADPH act as a constraint for the H2 production.

Although some researchers like Mèlissa Cano and her team (Cano et al, 2014) were able to produce an oxygen tolerant Ni-Fe hydrogenase Synechocystis sp. PCC 6803 strain using directed mutagenesis, the Ni-Fe hydrogenase oxygen intolerance is still quite a major barrier for the production of H2 in Synechocystis sp. PCC 6803.

From the point of view of the metabolic engineering, the next steps on the enhancement of H2 production in Synechocystis are based on the redirection of the electron flow through these hydrogenases, while overcoming the inhibition produced by the oxygen. To make this possible, it is necessary to develop a fully understanding of what the Electron Transport Chain is, and how it behaves.

3.1 The Electron Transport Chain

The electron transport chain is a concatenation of protein complexes and molecules capable to transport electrons from a high energy state to a low energy state, producing reducing power and a proton motive force (pmf) as a result. In cyanobacteria, contrastingly from higher plants, the ETC gathers electrons from two distinct sources: photosynthesis and respiration (Vermaas, 2001).

The ETC is harbored into the thylakoid membrane of the cyanobacteria (Fig. 8) , where components from the respiratory and the photosynthetic chain are placed contiguously, and in contact with a cytoplasmic side and a luminal side, in which protons are pumped due to the action of the electron transport.

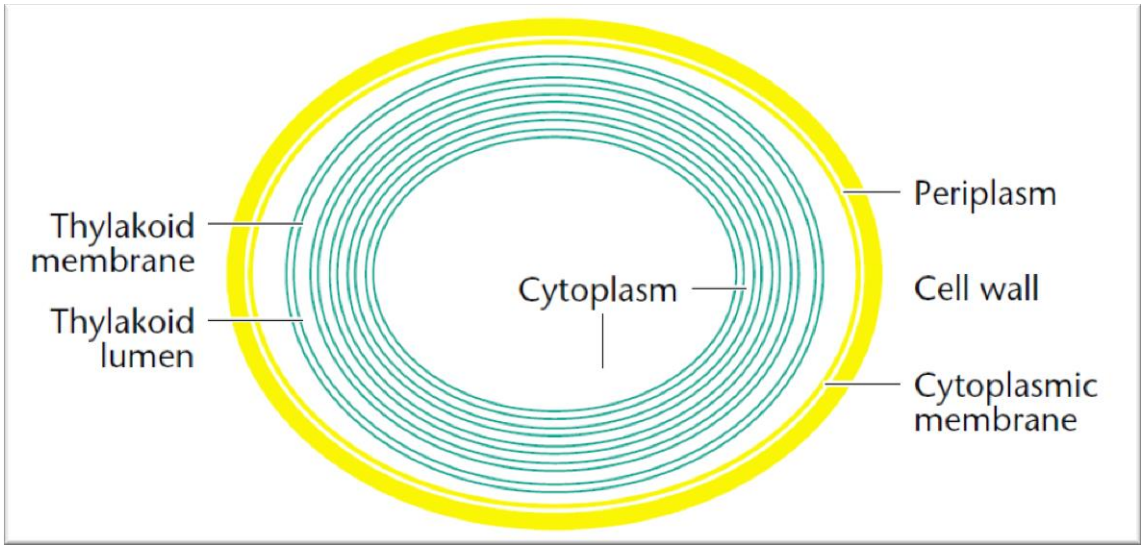

Figure 8. *Compartmentalization of cytoplasmic and thylakoid membrane in the interior of Synechocystis sp. PCC 6803*

The ETC bases its action in the transport of electron from a low energy state to a high energy state in the Photosystem II by the energy provided by the light (P680), and again to a low energy state and a re-energization in the Photosystem I, again with light energy (P700).After that, the electrons suffer another energy decay, to finally form part of reducing power to the cell (an excess of electrons in the ETC can be dissipated by the many electron valves present on it). This behavior can be graphically described using the so called "Z-scheme", graphical representation named after its particular shape of a laying Z (Fig. 9):

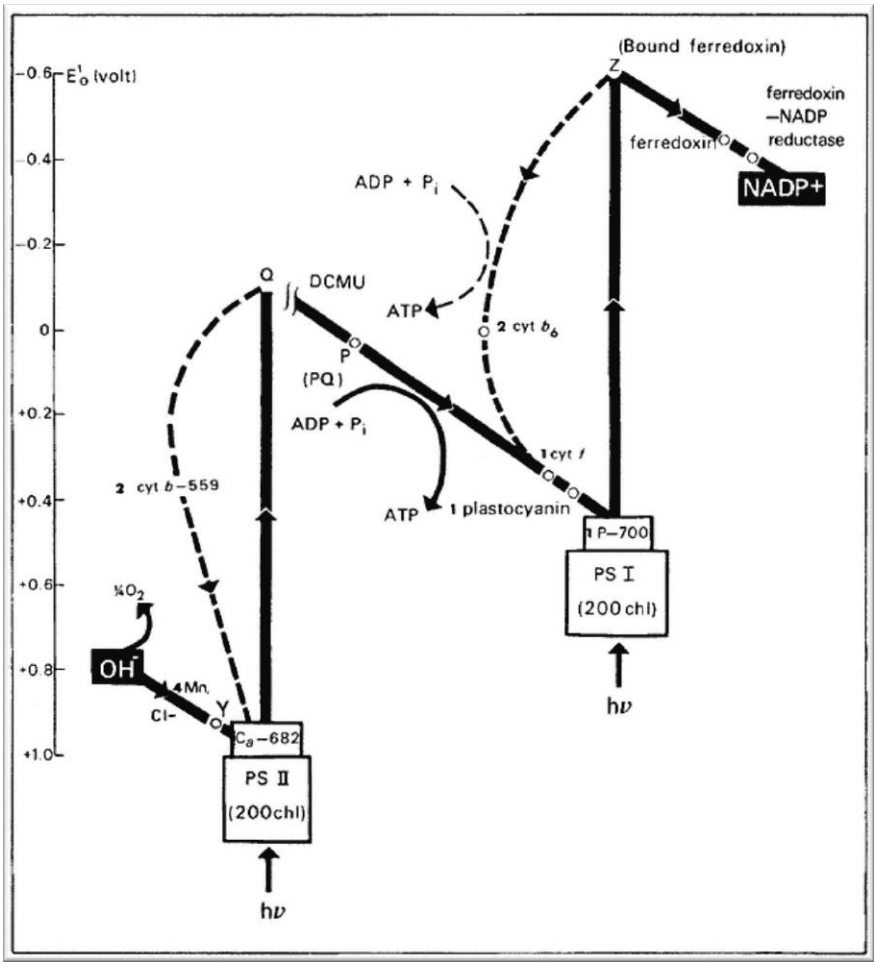

***Figure 9**. Z-scheme. The scale on the left represents the redox potential in Volts.*

The electrons entering the ETC of Synechocystis sp. PCC 680, differently from the majority of the photosynthetic organisms, have two different origins: a photosynthetic one, when electrons come from the splitting of water in the Oxygen Evolving Complex; or a respiratory one, when electrons come from the oxidation of succinate by the Succinate Dehydrogenase (SDH) coming from the TCA. Despite both origins have a major importance on the behavior of the ETC, in this project we only worked with those belonging to the photosynthetic chain, and so, we not reviewing the exclusive components of the respiratory chain

The ETC is composed by an enormous quantity of molecules and proteins, but we can organize them in several protein complexes included in the thylakoid membrane, by their order of action[1]:

***Table 1**. Major protein complexes of the photosynthetic electron transport chain*

Complex	Gene designation	Major proteins	Function
Photosystem II	*Psb*	D1,D2, CP43, CP47, PsbO	Light-induced water splitting (OEC) and PQ reduction
Cytochrome b6f	*pet*	Cyt b6, cyt f, Rieske subunit IV	PQH2 oxidation and PC reduction. Responsible of the cyt b6f cycle
Photosystem I	*psa*	PsaA, PsaB	Light-induced PC oxidation and Fd reduction
Cythochrome oxidase	*cta*	CtaC, CtaD, CtaE	Cyt c oxidation and O2 reduction
Cytochrome bd	*cioB*	CydA, CydB, CydX	PQ oxidation and O2 reduction

Apart from these complexes, the ETC is assisted by a variety of electron carriers:

***Table 2.** Electron carriers of the photosynthetic electron transport chain*

Electron carrier	Function
Plastoquinol	Act as a central pool of electrons, receiving electrons from both linear and cyclic transport. PSII oxidation and cyt b6f reduction
Plastocyanin	Cyt b6f oxidation and PSI reduction
Ferredoxin	PSI oxidation and FNR reduction. Provides electrons for N2 assimilation.
NADP/NADPH	Ferredoxin oxidation. Act as reducing power for many metabolic routes

There are also a number of enzymes, which while not being big protein complexes, are also vital for the functioning of the ETC[2]

***Table 3.** Electron transport enzymes of the photosynthetic electron transport chain*

Enzyme	Gene designation	Function
NADPH dehydrogenase I	*ndh*	NADPH oxidation and PQ reduction
Ferredoxin-NADP oxidoreductase	*peth*	Ferredoxin oxidation and NADP reduction
Flv 1-3	*flv*	Ferredoxin oxidation and O2 reduction (Mehler reaction)
PGR5	*pgr5*	Ferredoxin oxidation and PQ reduction

However, for a full comprehension of how the ETC works, a brief overview is not enough. For developing a mechanistic model, it is necessary to make a general review, focused more on all the mechanisms that take place in the ETC, rather than focused on structural, genomic and proteomic parameters more typical of a traditional biotechnological approach.

1,2 Data extracted from CyanoBase (http://genome.microbedb.jp/cyanobase/)

Photosystem II (P680)

Photosystem II consists of a dimeric protein complex, formed by two monomers, each one with 16 integral membrane subunits and three luminal membranes (Fig. 10) (Ferreira et al., 2004). The D1 and D2 subunits form the reaction center of the PSII, and are the major responsible of the electron transfer reaction through the PSII. This photosystem also present the CP43 and CP47 region, where the chlorophyll responsible of light-induced electron excitation and charge separation, P680 is bound (14 and 16 Chl respectively). The PSII also harbors the OEC, a cubane-like Mn_3CaO_4 cluster responsible of the breakage of water into protons, molecular oxygen and electrons, which will enter the ETC. These electrons are conducted throughout the whole photosystem to the QA/QB site, where they will be transmitted to the plastoquinol.

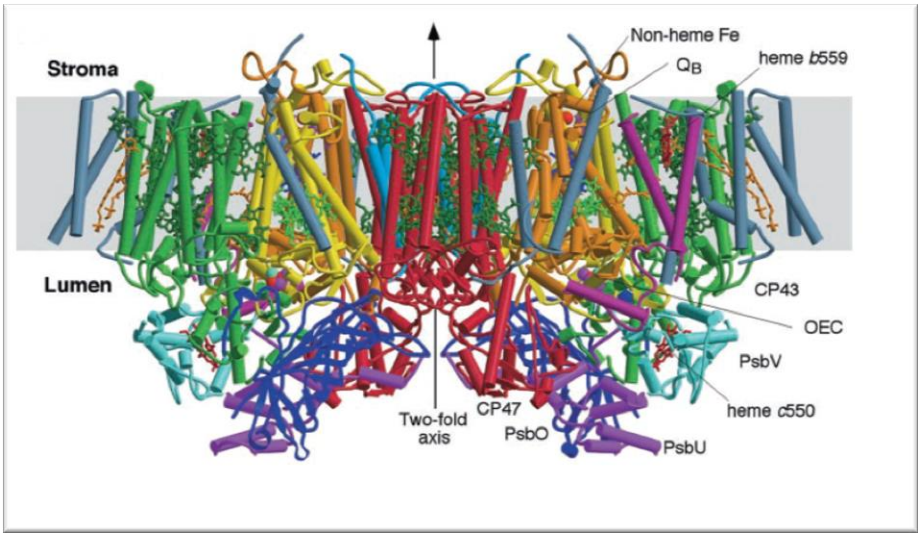

***Figure 10**. 3-D structure of the PSII dimer.*

The Photosystem II is responsible for three functions in the ETC: the water splitting at the Oxygen Evolving Complex (OEC), which releases the electrons that are later conducted through the ETC; the excitation of electrons by a light-induced charge separation mediated by the chlorophyll antennas of the CP43 and CP47 which will provide the electrons from the OEC the necessary energy to be conducted to the PSI, and the reduction of plastoquinol in the QA/QB site, which allows the electrons to travel from the Photosystem II to the Cytochrome b6f:

Water Splitting

The Oxygen Evolving Complex (OEC) is formed primarily by a Mn_3CaO_4 (Fig. 11) cluster linked to a tyrosine residue, and is the most oxidizing substance known by biology, with an Em about one volt (Antal and Kovalenko, 2013). The functioning of this complex, as explained by Kok (Kok et al., 1970), is based in a cycle of five states of oxidation (S_0-S_1-S_2-S_3-S_4). As stated by this model, the OEC behaves as a linear four quantum process, in which four consecutive quantum excitation produced by light incidence add consecutively four charges to the OEC, driving it from S0 to S4. Once the S4 state is reached, the OEC is able to break two water molecules, gathering four electrons and leaving four protons and a molecular oxygen. The electrons are transmitted to the oxidized form of a TyrZ residue, which connects the OEC with the PSII antennas; the OEC returns to the S0 state, restarting the cycle. The protons are released into the lumen, contributing with the proton motive force.

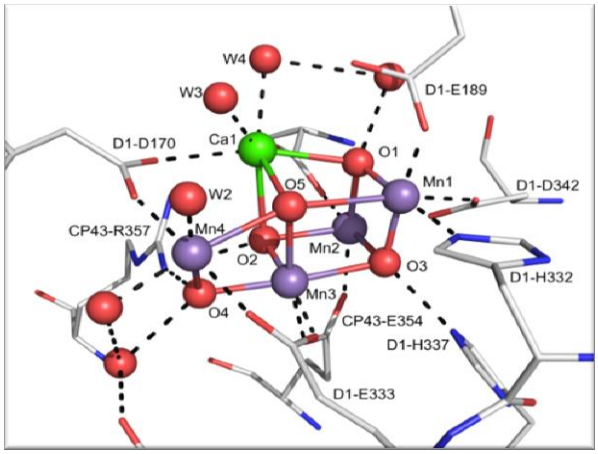

***Figure 11**. X-Ray crystal structure of the Mn cluster of the OEC.*

Charge separation

The chare separation on PSII is based on the action of a pair of chlorophylls known as P_{D1} and P_{D2} (Fig. 12) (Cardona et al., 2011)When the light falls upon these pigments and the other pigment of the PSII, an electron from the outer valence of the P_{D1} is excited and transported to a higher energy state. This excitation makes possible the formation of the P_{D1}^+/Ph_1^-, this means, the electron is transmitted from the chlorophyll to a pheophytine residue that will continue the chain. The outcome of this charge separation is the formation of a P_{D1}^+ form lacking an electron in its outer valence. This electron is replenished with that one coming from the TyrZ of the OEC.

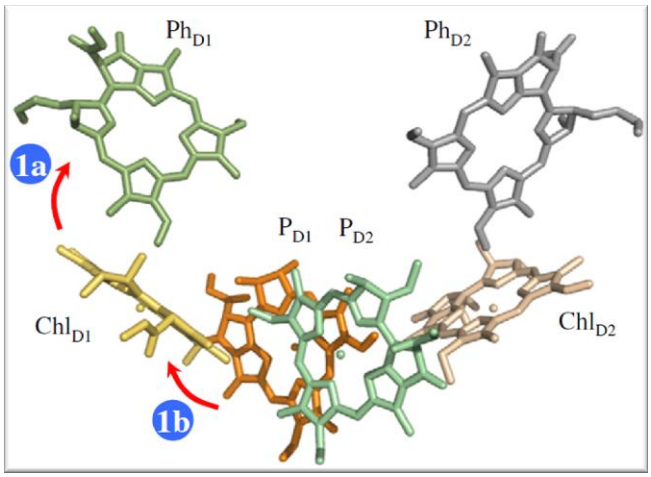

***Figure 12**. X-ray crystal structure of the P_{D1}/P_{D2} pair and electron transmission to pheophytine.*

The charge separation provides the electrons with the sufficient energy to cross through the ETC to the PSI. This process means a huge shift on the redox potential of the chlorophyll, switching from Em= 1.125 V to Em= -0.705 V (Antal and Kovalenko, 2013).

Reduction of plastoquinol

Once the Ph is reduced with the electrons comes from the charge separation, the next and last step taking place in the PSII is the reduction of plastoquinol. The electron coming from

the pheophytine is conducted following a redox potential positive gradient to the Q_A, a firmly bound plastoquinone. The electron is transmitted the, via a non heme Fe group, to the Q_B site of PSII. It is in this site where the PQ binds to the PSII and gets reduced. The PQ binds with the reduced Q_B site, forming a pair Q_B^-/PQ. The Q_B^- is reduced again, giving the Q_B^{2-} form; is in this state, when the Q_B^{2-} gets protonated, forming QBH2, and leaving the PSII as PQH2. Finally, another PQ binds to the Q_B site and restarts the cycle (Fig. 13).

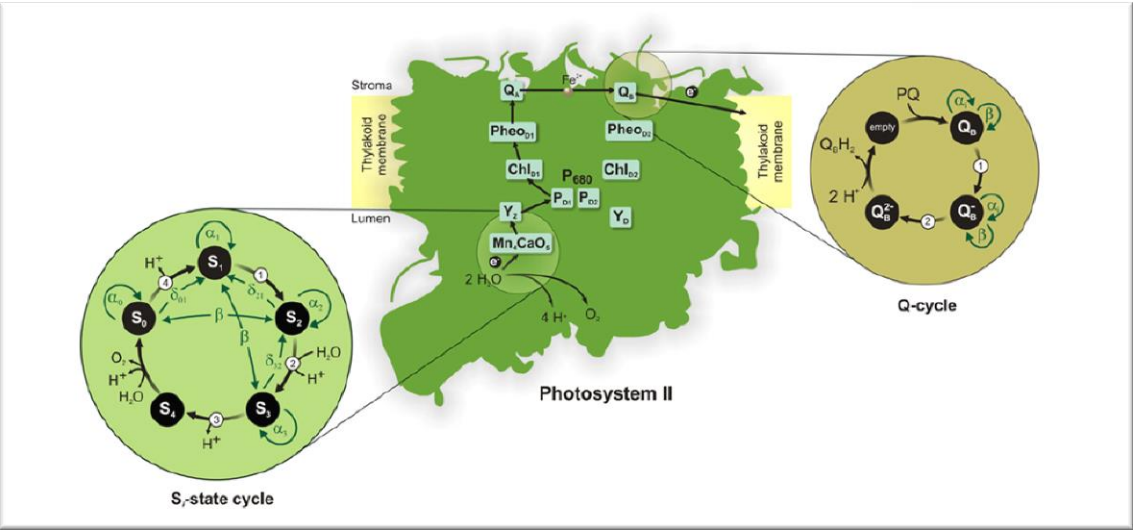

***Figure 13**. Electron path in the PSII, from OEC to PQH2, including the Kok cycle (left) and the Q_B-cycle (right).*

Plastoquinol pool

The plastoquinol is a lipophilic, membrane-bound electron carrier that can accept two electrons and two protons to form PQH2, which can donate its electrons to the cytochrome b6f, one to the high energy chain, and one to the low energy chain. Apart from that, the PQ is also participating in many other reactions, acting as a core electron pool of the whole ETC.

- Gathers the electrons coming from succinate oxidation in respiration
- Receives the electrons coming from the cyclic transport, both short (Fd) and long (NADPH) cycles.
- Completes the PQ cycle in the cytochrome b6f
- Alleviates the energetic state of the ETC by donating electrons to cytochrome bd.

Due to the role of the PQ pool as the center of many reactions involved in the ETC, the redox state of the PQ pool can be even used as an indicator of the homeostatic state of the cell (Schuurmans et al, 2014).

Cytochrome b6f

The cytochrome b6f is an integral membrane protein complex which occupies an electrochemically central position into the ETC. Cytochrome b6f is formed by 8 different

subunits (Baniulis et al, 2008): two cytochromes, cyt f and cyt b6; ISP subunit, which engulfs the Rieske protein with the 2Fe-2S cluster, and five other subunits(suIV, PetG, PetM,PetL,PetN) (Fig. 14).

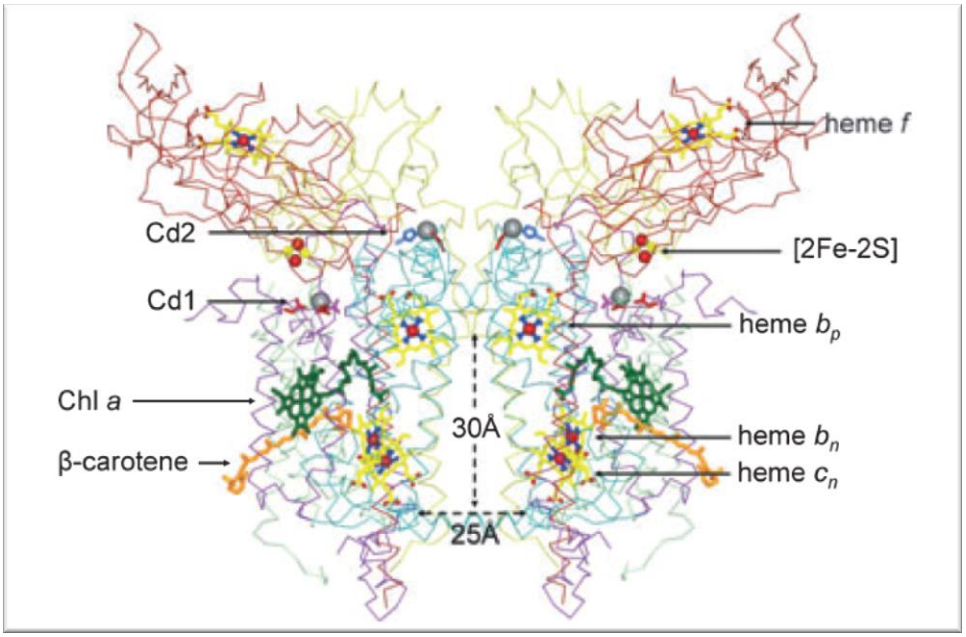

***Figure 14**. X-ray crystal structure of the cytochrome b6f.*

The cytochrome b6f is responsible of two different electro transport pathways, based on the action of 4 four main components:

- A high potential chain, formed by the known as Rieske protein, which includes a high potential 2F-2S cluster; and the cytochrome f.
- A low potential chain formed by two noncovalent bound b-type hemes, b_p and b_n., situated in the. This low potential chain is responsible of the cytochrome b6f cycle (Mitchell, 1975).

So as seen, there exist two different pathways of electron transport, a high potential one, and a low potential one:

<u>High potential chain (Linear transport)</u>

This pathway is part of the main linear transport of electrons through the ETC. When the PQH2 arrives at the ISP subunit through the cytoplasmic side of the cytochrome b6f, it binds to the Rieske protein, giving an electron to the 2Fe-2D cluster. In this step, the two protons from the PQH2 are released into the lumen. The ISP subunit suffers a hypothetical (Zhang et al. 1998) conformational change, and proceeds to give the electron to the cytochrome f, which later gives the electron to the plastocyanine, a noncovalent bound electron carrier.

As a consequence of this process, a non-confirmed form of plastoquinol is formed, the semiplastoquinone (SPQ) (Cape et al., 2007), which consists of a plastoquinol with no protons bound and an extra electron. This

Low potential chain (Cyclic transport)

The low potential chain is responsible of the known as Q-cycle, a process in which, using the electrons provided by the PQH2, the cytochrome b6f is able to pump protons into the lumen at a zero energy cost, since at the end of the cycle, a new PQH2 molecule is generated (Fig. 15). This cycle consists of two phases:

1. Phase 1. In this step of the cycle, the SPQ coming from the Rieske protein binds the heme b_p group of the cytochrome b6f, leading to an electron transmission between the two molecules. This electron will be later transmitted throughout the cytochrome across the membrane to the heme b_n group. At this point, a PQ molecule binds the at the heme b_n side, receiving an electron and becoming a SPQ molecule.

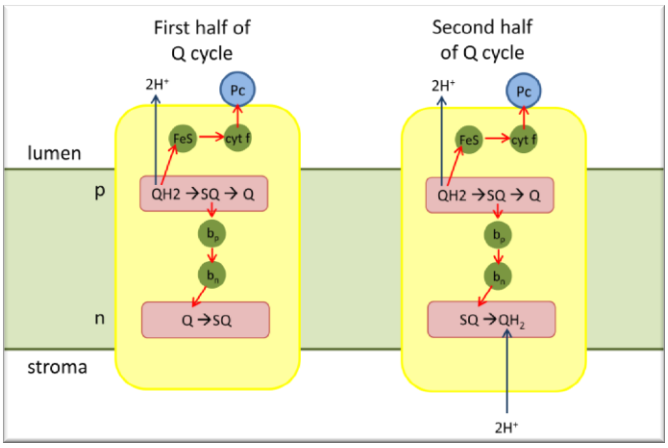

***Figure 15**. Scheme of the Q-cycle in cyt b6f*

2. Phase 2. In this step a similar process takes place. The electron coming from the SPQ on the formed on the Rieske protein travels across the cytochrome through the heme b and heme bn groups. At the end, this time the electron is transmited to a bound SPQ, regenerating a PQH2 that will enter again the cytochrome b6f, thus restarting the cycle.

This cycles increment the H+/e- ratio of the linear transport chain, since it allows pumping one more proton per electro going across the cytochrome b6f. This increases the pmf generated by the ETC, and therefore, improves the production of ATP at the ATP synthase.

Plastocyanin

The plastocyanin is a blue-copper protein highly conserved among cyanobacteria and other organisms such as E.coli and higher plants (Hervás et al. 1993). Plastocyanin has two roles in the ETC

a. Functions as an electron carrier between the cytochrome b6f and photosystem I.
b. Gives electrons to the cytochrome c in situations of light-induced stress.

Photosystem I

The PSI is a large membrane protein complex responsible of the second reeenergization of electrons in the ETC. It is composed by 12 different proteins, (PsaA, PsaB, PsaC, PsaD, PsaE, PsaF,PsaI,PsaJ, PsaK, PsaI, PsaM and PsaX), with 127 non-covalent bound cofactors

(Fig. 16) (Grotjohann and Fromme, 2005). From all these subunits, the most important are PsaA and PsaB, which are located in the core center of the PSI, harboring the majority of chlorophylls and carotenoids from the antenna system, as well as the most of the cofactors of the electron transport chain.

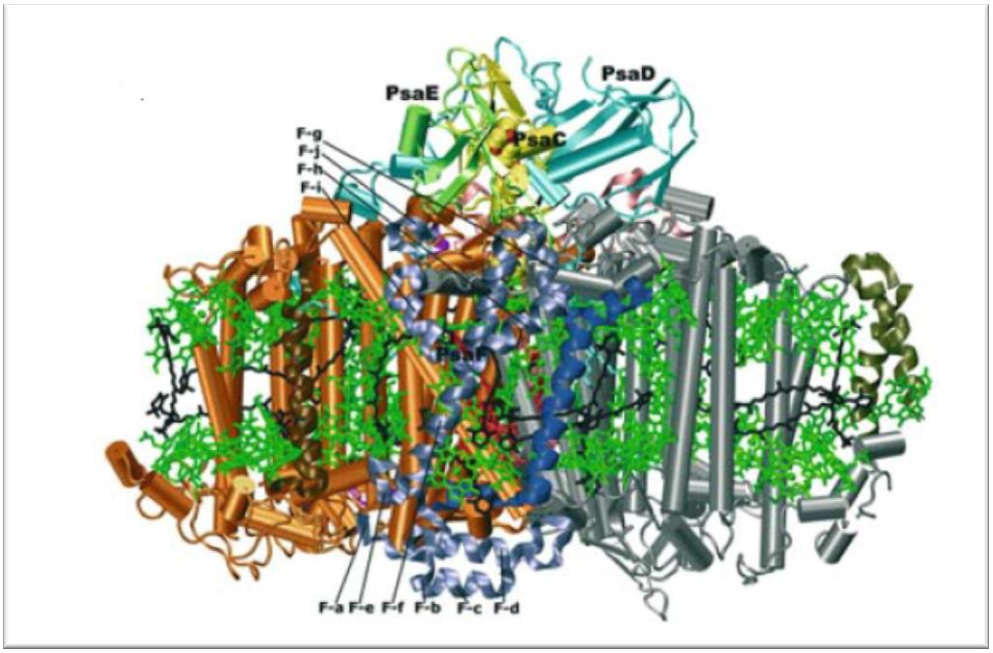

***Figure 16**. X-ray crystal structure of the Photosystem 1*

The P700 receives the plastocyanin in its luminal side, which donates the electron for the regeneration of the neutral P700 chlorophyll a form (P700 stands for the maximum absorption wavelength of this chlorophyll). Once in this state, the process of charge separation is based on the action of a small electron transport chain formed by six chlorophylls in three pairs (P700, A and A0) two pollyquinones (A1) and three 4Fe-4S clusters (F_X, F_A and F_B)

The process of charge separation and energy transfer is quite similar to that one from Photosystem II: when a photon hits the neutral form of P700, and electron from the outermost valence is excited and separated from this chlorophyll, leaving a $P700^+$ form (Hastings et al., 1995). The electron is then accepted by the first chlorophyll acceptor, A, which transmits the electron to the stable electron acceptor, A0. In this step, the electron is transferred to the pollyquinone A1 (Brettel, 1997), which transmits the electron through the three cofactors F_X, F_A and F_B (Fig. 17)(Ke, 2001).

Finally, the electron is transferred to the ferredoxin, docked in the acceptor site of the PSI by the action of the membrane extrinsic PsaC, PsaD and PSaE subunits of the photosystem (Barth et al, 1998).

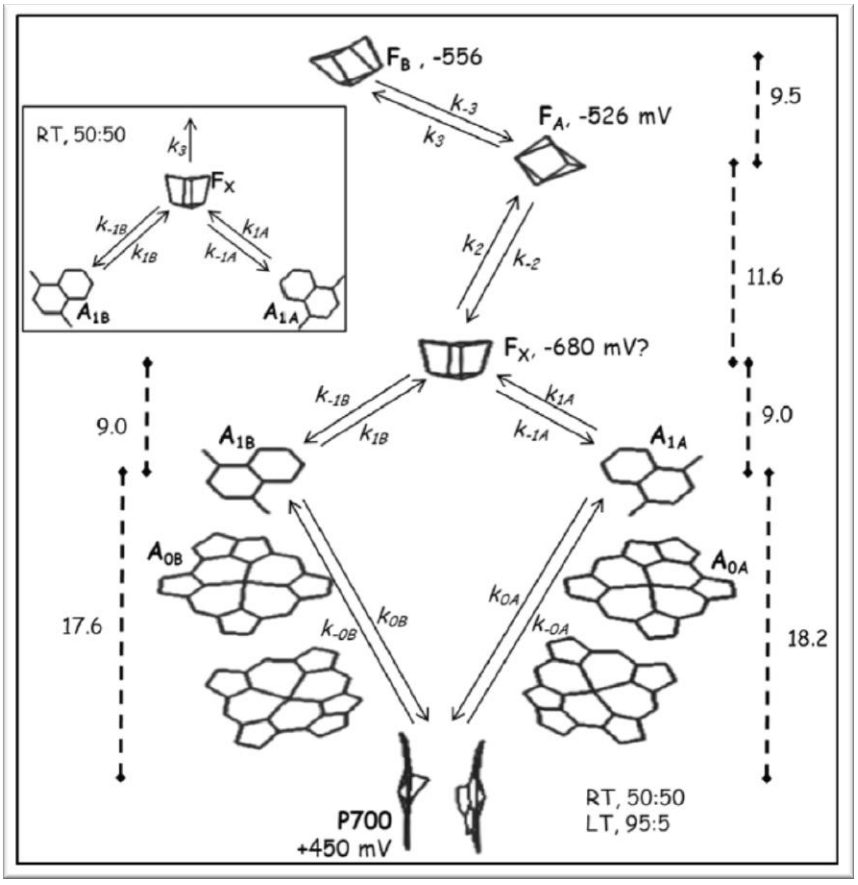

***Figure 17**. Scheme of the ETC of the PSI core. Distance between elements (Å) and redox potential (mV) of every component are indicated*

As a result of the action of PSI, the electron is energized from an Em= 440 mV to an Em = -440 mV, a total shift of one volt (Antal and Kovalenko, 2013).

Ferredoxin

Ferredoxin is a nonheme containing protein with an iron sulfur cluster 2Fe-2S (Lovenberg, 1963). Ferredoxin gathers the electrons from the acceptor site of the photosystem I, and distributes them amongst various routes related with the ETC and the general metabolism of the cell:

- In linear transport, ferredoxin donates electrons to the ferredoxin-$NADP^+$ oxidoreductase, an enzyme capable of that transmits electrons from the ferredoxin to the $NADP^+$.
- In short cyclic transport route, ferredoxin is the donor of electrons to PGR5, an enzyme that takes electrons from ferredoxin and gives them to plastoquinol.
- Ferredoxin can alleviate an light-induced energy stress in the cell by giving electrons to the Flv1-3 proteins (Mehler reaction).
- Ferredoxin provides the energy necessary for N assimilation (NO3->NO2; NO2->NH3).

Ferredoxin-NADP$^+$ oxidorreductase

The ferredoxin-NADP$^+$ oxidoreductase or FNR is a flavoenzyme that acts as a bridge between ferredoxin and NADP$^+$ (Karplus, 1991). For reducing a NADP$^+$ to NADPH, two ferredoxins are required. These ferredoxins give their electrons to the FAD prosthetic group of the FNR, which switches first to the neutral Flavin semiquinone, and then to a fully reduced form. When FNR is fully reduced, it gives both electrons to NADP$^+$, producing NADPH and releasing two oxidized ferredoxins.

In FNR, electrons are transferred from two molecules of an one-electro donor to a single molecule of a two-electron acceptor. Due to this particular nature, FNR is classified into the group of the so called dehydrogenase-electron transferases (Hemmerich and Massey, 1977).

NADP$^+$/NADPH

The nicatinamide adenine dinucleotide phosphate or NADP$^+$/NADPH is a dinucleotide that acts a reducing power and electron donor for many metabolic routes present on the cell. NADPH is generated by the action of FNR, which donates two electrons from two ferredoxins in this acceptor site. When the reduced form is formed, two protons join this form to give the final species.

NADPH represents the final stage of the linear ETC, where the two electrons from the water splitting, travelling across many membrane complexes, electron carriers and enzymes, finally adopt a form in which they can be exploited by many other metabolic processes.

Into the ETC, NADPH also participates in the long cyclic transport via the NDH-1 enzyme, used by the cell to generate extra pmf and improve the ATP production.

3.2 Non-linear components of the ETC: cyclic transport, oxygen evolution and electron valves

Apart from the main linear ETC route, there are other accesory routes that help the cell to increase the ATP production per electron inside the photosynthetic apparatus, or to prevent photsynthetic damage by evolving oxygen in a way to alliviate the excess of electrons (Kramer and Evans, 2011) .

Cyclic transport

The cyclic transport around PSI is used by the cell to increase H+ pumping into the lumen, and thus, ATP production (Kramer). There exist two main cyclic routes of cyclic transport around PSI:

- Short route: PGR5

The short route is based on the electrons provided by the ferredoxin, which are transmitted into the plastoquinol pool via PGR5. PGR5 is a recently discovered protein with a mass of 10 KDa, which is able to take the electrons from ferredoxin and give them again to plastoquinol, closing a cycle around PSI.

The precise function of PGR5 is not totally understood yet, but it seems like PGR5 develop a photoprotection activity of the PSI (Munekage et al, 2002).

- Long route: NDH-1

The long cyclic transport route is based on the action of the NADPH dehydrogenase Type 1, a protein complex formed by 11 subunits (NdhA to NdhK). NDH-1 is capable to take the electrons from NADPH and transmit them to the plastoquinol pool.

In a different way from PGR5, NDH-1 is also capable to pump two protons into the lumen, halving the rate of cyclic electron transport needed to balance the ATP/NADPH ratio. The expression of NDH-1 is low under nonstressed condition, only showing strong activity under environmental stress (Zhang et al., 2004).

Oxygen evolution and electron valves

Around the linear ETC are several electron valves which function is to relief light-induced stress conditions, by evolving oxygen to water giving the electrons stored in the various electron carriers of the ETC. The main control pathways are:

- Mehler reaction (Flv1-3)

The Mehler reaction is a process in which the oxygen is evolved to water by the electrons donated by ferredoxin. It is mediated by the FLv1 and Flv3, a pair of flavofiiron proteins that donate electrons to O2 without production of reactive oxygen species.

Thus, the Flv1/Flv3 heterodimer maintains the redox balance of the ETC and provides protection for PSI under fluctuating light conditions (Allahverdiyeba et al., 2013).

- Cytochrome c and cytochrome bd oxidases

The cytochrome c and cytochrome bd oxidases are protein complexes capable to take electrons from plastocyanin and plastoquinol respectively, and use them to reduce oxygen into H2O.

Both cytochromes work in a similar pattern, but their function is distinct:

  - The function of cytochrome c oxidase is to act as a terminal electron sink under conditions of low PSI activity, or to prevent over reduction of soluble redox carriers (Howitt and Vermaas, 1998).

- The function of the cytochrome bd is to prevent to over reduction of the plastoquinol pool in a situations of high light intensities or malfunction of cytochrome b6f (Mogi and Miyoshi, 2009).

3.3 ATP synthase: components of the protonmotive force

The F_0F_1-ATP synthase is an ubiquitous membrane bound enzyme (Fig. 18) which catalyzes the synthesis of ATP from ADP and inorganic phosphate, at the expense of electrochemical proton gradient across the membrane generated by the photosynthetic electron transport (Imashimizu et al., 2011).

The ATP synthase is composed by two main elements:

- F_0. The F_0 component is an membrane integral part which acts as a proton channel through the thylakoid membrane.
- F_1. The F_1 component is composed of three α subunits, three β subunits, one γ, one δ and one ε subunits. The γ, δ, and ε subunits regulate the activity of the ATP synthase and connect F_0 with α and β subunits, which adopt a rotor-like form. When protons travel through the F_0 proton channel, they generate an energy which is used to rotate the rotor like structure of F_1. This rotation is employed, in a complex cycle, to generate ATP from ADP and Pi.

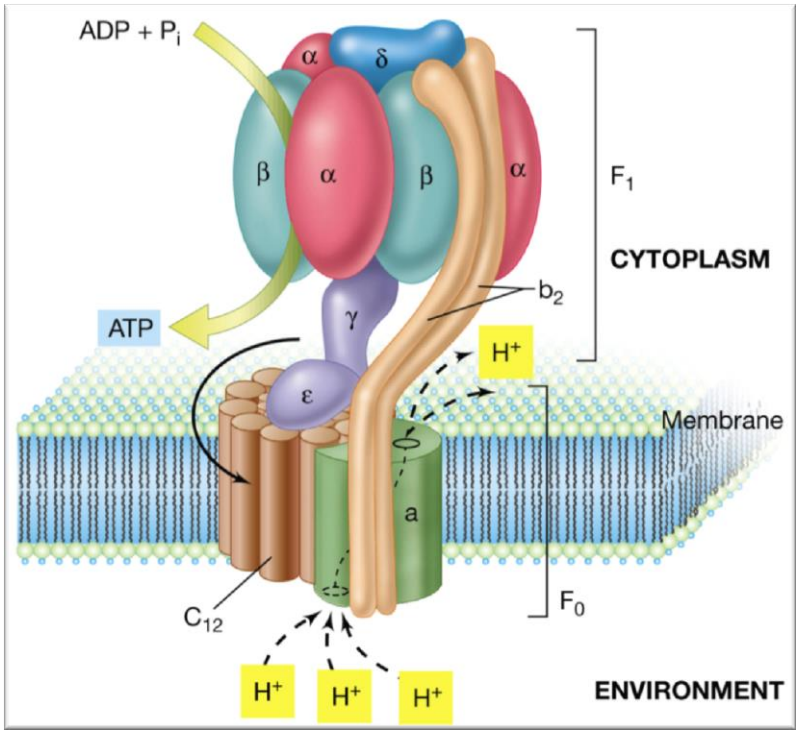

***Figure 18**. Structure of the F_0F_1-ATP synthase*

The driving force for the ATP synthesis is the tendency of protons to escape from the lumen to the cytosol through the F_0 channel, which is known as the protonmotive force. This driving force consists of two equivalent components:

- Electrochemical potential. The electrochemical potential is the voltage difference across the thylakoid membrane caused by the difference of charge between both sides. This charge depends on the nature of the ions at each side of the membrane (positive or negative), and the concentration of each species. In Synechocystis sp. PCC 6803, the main species influencing the electrochemical potential are Ca^{2+}, Mg^{2+}, K^{+} and Cl^{-}, plus the influence of both H^{+} and OH^{-} ions.

  $$Total\ Charge = F * (2[Ca^{2+}] + 2[Mg^{2+}] + [K^{+}] + [Cl^{-}] + [H^{+}] + [OH^{-}])$$
  (Equation 1)

  The electrochemical potential is thus computed as the difference of charge between the luminal and the cytoplasmic side, divided by the capacitance of the membrane:

  $$\Delta\Psi = \frac{Total\ Charge_{\ lumen} - Total\ Charge_{\ citoplasm}}{Membrane\ capacitance}$$ (Equation 2)

While there are several ion channels across the thylakoid and the cell membrane (Checchetto et al, 2013), the generation and control of the protonmotive force is majorly controlled by the next component.

- pH gradient. The generation of the pH gradient is the major objective of the whole ETC previously reviewed. The transport of electrons across the ETC leads to a proton pumping into the lumen, which increases its pH, and thus, the pH gradient between lumen and cytoplasm; the higher the gradient, the bigger the protonmotive force is.

  However, depending on the necessities of the cell, the electrons can be transported across the previously seen routes, varying the H^{+}/e^{-} ratio:

  - Linear transport with b6f cycle. The b6f cycle adds two more protons pumped into the lumen per water molecule split than the linear transport without this cycle.

  - Cyclic transport around the PSI. These routes add suppose eight protons pumped per water molecule split, six from the normal linear transport, and another two from the electrons going again through the cytochrome b6f.

  - Transport with Mehler reaction end. This route supposes the same proton pumping than linear transport, since the only difference is the final acceptor of these electrons (O2 instead of NADP).

  - Transport across the cytochrome c. Similar to the Mehler reaction, it provides the same yield as the linear transport.

- Transport across the cytochrome bd. This is the route which pumps fewest protons into the lumen, because they aren´t able to reach the cytochrome b6f. Only two protons per water molecule split are pumped.

So, assuming that the ratio between protons going across the ATP synthase and ATP produced is 4.67, the yield of each electron transport route can be summed up in the next table:

Table 4. *ATP yield per water molecule split in the OEC depending on which pathway is used*

Route	PSII photons	PSI photons	Protons pumped	ATP produced
Linear transport with cyt b6f cycle	2	2+2	6	1.28
Cyclic transport around PSI	2	2+2+2	8	1.71
Mehler reaction	2	2+2	6	1.28
Cytochrome c	2	2+2	6	1.28
Cytochrome bd	2	-	2	0.42

3.4 The bidirectional Ni-Fe hydrogenase

The bidirectional Ni-Fe hydrogenase (Hox) catalyze the reduction of protons to hydrogen and the reaction viceversa, when the electrons stored in hydrogen are needed to supply other metabolic routes. It is composed by five subunits (HoxE, HoxF, HoxU, HoxY and HoxH), with HoxEFU forming the module that interacts with NADPH and mediates the electron transfer to the hydrogenase part, formed by HoxY and HoxH and holding the active Ni-Fe site.

Hox can take electrons from NADPH and ferredoxin (also from NADH, which is not reviewed here). While NAD(P)H are poor electron donors in this case, and lead to a very little production of H2, ferredoxin is quite a better donor, due to its higher redox potential (Em Fd= -440 mV , Em NAD(P)H= -320 mV; Em H+/H2=-414). Therefore, much less concentration of ferredoxin is needed to activate the hydrogenase activity than the concentration needed of NADH (requires a Fd_r/Fd_{ox} ratio of 0.1-0.3, versus a NADH/NAD+ ratio close to 1000). Recent studies have, effectively, proved that ferredoxin acts as the main electron donor to the Ni-Fe hydrogenase activity (Gutekunst et al, 2014).

Hydrogenase is essential for survival under mixotrophic, nitrate limiting conditions, in which the nitrate reduction is impossible to achieve, and the cell requires an alternative electron sink. So, the Ni-Fe hydrogenase functions as an electron sink for reduced ferredoxin under these specific conditions. Studies with nitrate assimilation lacking activity have showed that the production of H2 increases in the mutant strains unable to reduce nitrates (Gutthann et al, 2006).

The [Ni-Fe] hydrogenase present in Synechocystis sp. PCC 6803 is quite intolerant to the oxygen produced in water splitting. In addition, the oxygen acts a as a competitor for the electrons, in a same patterns the nitrogen and the carbon do; this makes that the

hydrogenase is only active under microoxic or anoxic conditions, where the hydrogen is the only available electron sink and no inhibition takes place.

As we have seen across this report, the electrons transmitted through the ETC are used and stored into several electron sinks: NADPH that is sent both to the Calvin cycle, nitrate assimilation thanks to the electrons stored in ferredoxin, oxygen evolution via electron valves, and lastly, H2 production.

As metabolic engineers, we are capable of playing with the metabolic routes present on the microorganisms, redirecting the metabolic fluxes wherever our interest is focused. In this case, the goal for metabolic engineers is to redirect the electron flow of the ETC into the reduction of protons to form H2 using only light as energy source. It is clear, that the major challenge for the next years is using genetic engineering to maximize and get a sustained electron flow into the hydrogenase, while preventing its inactivation by oxygen by engineering more oxygen-tolerant hydrogenases.

To achieve this goal, systems biology emerges as a powerful tool: instead of constructing a wide range of mutants to test them *in vivo*, which is slow and expensive, an *in silico* approach can help as to analyze all the possible beneficial modifications in faster, cheaper and more efficient way. The model introduced in the next pages is one of the several attempts developed by teams across the world to provide the scientific community with a photosynthesis model of Synechocystis sp. PCC 6803 that can help them to accomplish their objectives.

4. Applying Systems Biology: A model for the Synechocystis sp. PCC 6803 electron transport chain.

Building a model for the photosynthetic electron transport chain of Synechocystis sp. PCC 6803 implies the collision of three different worlds: the informatic, the mathematic and the biotechnological one. This entails that there are many aspects of each world that cannot be totally respected, if we want everything to work together. Many considerations had to be made in the development of this model, and many elements had to be discarded. Nevertheless, during the construction of the model, there were three pillars around the model were built:

- **Simplicity**. The previous review of the ETC is just an extremely simple overview of all the processes that are really taking place there. To precisely model every reaction taking place in the photosynthesis, is, at the time, not only a gargantuan task, but also an impossible one, since the tools and experiments required to know every reaction, every kinetic parameter, have not still been developed.

For that reason, many reactions were not included in this model, and many others have been simplified into a manageable form; there have even been important processes, such as the non-photochemical quenching in the PSII, that have not been included in this version of the model
This does not mean that the model is imprecise or incomplete, because although not every reaction is included in it, the global picture of the ETC has been captured and modelled.

- **Robustness**. Though simple, the model has to respect the laws of the thermodynamic; this means, the energy entering the system (the electrons entering the PSII) has to be equal than the energy leaving the system (the electrons leaving via carbon, nitrogen, oxygen and hydrogen output) in the equilibrium.

- **Saturable rate equations.** There exist many models that are based on linear rate equations like the Mass Action Law (MAL) (Vershubskii et al, 2014). Although simple and malleable, we think that this kind of equations is unable to provide precise results in the field on the biological systems. Because of that, we opted to introduce saturable rate equations to build the model, as we think these equations can fit much better what's happening in real life.

4.1 Reactions rate equations employed in the model

The model here explained is capable of monitor the rate of 37 different reactions and the concentration of 45 different molecules, complexes, enzymes and ions. The model follows the structure of an Ordinary Differential Equation (ODE) system; this means, each one of the 44 different molecules concentration is the sum of the rate of the reactions in which the molecule participates, integrated by a specific given time.

As it was previously said, one of the goals of this model was to include saturable rate equations. There exist several examples of these equations, such as Convenience Kinetics (CK), Ping-Pong Mechanism (PPM), etc. Heiske discussed the performance of both linear and saturable rate equations simulating the reaction rate of the NDH-1 complex (Heiske et al., 2014). They concluded that saturable rate equations fitted much better the reaction rates obtained from *in vivo* experiments, and amongst these equations, the Extended-Reversible Henri-Michaelis-Menten equation (ER-HMM) was the one that better results gives when simulating the activity of NDH-1. Hence, we decided that the model would be based on the Michaelis-Menten kinetics.

The basic equation employed for this model is a developed form of the ER-HMM equation used by Heiske.

$$A^- + B \rightarrow A + B^-$$

$$v = \frac{v_{max}\frac{A^- \; B}{K_{A^-}K_B} - \frac{1 \; A \; B^-}{K_E K_A K_{B^-}}}{\left(1+\frac{A^-}{K_{A^-}}+\frac{A}{K_A}\right)*\left(1+\frac{B}{K_B}+\frac{B^-}{K_{B^-}}\right)} \quad \text{(Equation 3)}$$

A and B are the substrates of the reaction, while C and D are the products. K_A, K_B, K_C and K_D are the Michaelis-Menten constants for A, B, C and D respectively.

K_E is the equilibrium constant of the reaction. It is calculated the following way:

$$K_E = e^{\frac{-\Delta G}{RT}} \quad \text{(Equation 4)}$$

$$\Delta G = -nF\Delta E \quad \text{(Equation 5)}$$

$$\Delta E = Em_B - Em_A \quad \text{(Equation 6)}$$

ΔG is calculated based on the product of the difference between the midpoint redox potentials of the electron acceptor (E_B) and the electron donor (E_A), the number of electrons transferred in the reaction, and the Faraday constant.

While this equation was used for most of the reactions of the model, other variants of the MM kinetics were used:

- Extended Michaelis-Menten equation (E-MM)

$$v = \frac{v_{max}AB}{\frac{1}{K_A K_B}+\frac{A}{K_B}+\frac{B}{K_A}+AB} \quad \text{(Equation 7)}$$

  This equation was used for non-reversible, two substrate reactions.

- Standard Michaelis-Menten equation (MM)

$$v = \frac{v_{max}[S]}{K_m+[S]} \quad \text{(Equation 8)}$$

  This equation was used for reactions with an only substrate.

Other specific reactions have their own specific rate equations, which will be later discussed in this same report.

4.2 Molecules and reactions in the model

As it was previously said there is up to are 45 molecules, enzymes, subunits and protein complexes, (taking in account both reduced and oxidized forms) participating in 37 different reactions (Fig. 19). By means of space, we are not discussing here every reaction.

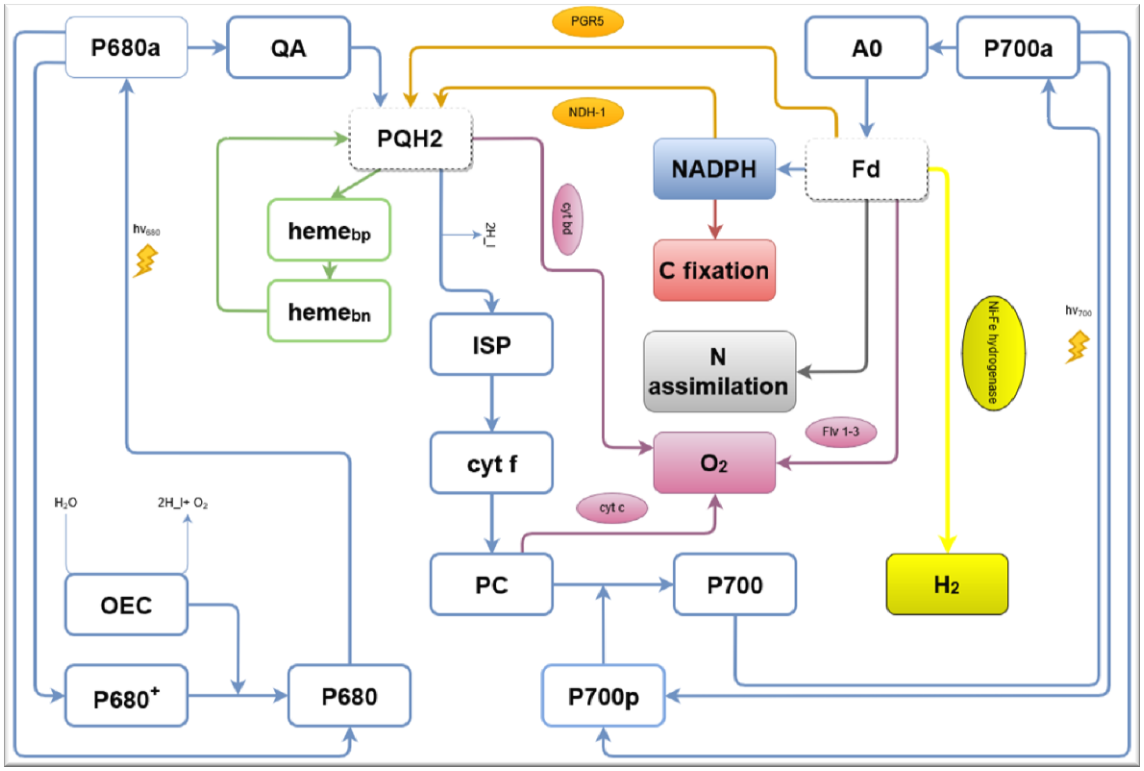

***Figure 19**. Diagram of electron fluxes included in the model. **Blue color** represents linear electron transport; **green color** represents the cytochrome b6f cycle; **orange color** represents cyclic transport around PSI; **purple color** represents oxygen reduction; **red color** represents carbon fixation; **grey color** represents N assimilation; **yellow color** represents hydrogen synthesis. ATP synthesis and ion fluxes are not represented here.*

Tables with the molecules, reactions and kinetic constants of the model, including the stoichiometry of the reactions; as well as all the equations used in this model, are included in Supplementary Files. In this report we are only discussing those parts of the model that required special considerations:

- **Light induced reactions**

There are three light-driven reactions in the model: water splitting at OEC, excitation of P680, and excitation of P700. The photons does not behave like the other molecules of the model, so they can´t be modelled only as another component of a Michaelis-Menten equation. However, there is at the moment very few models of light induced reactions, and these are too complex for the level of simplicity we wanted to keep in this model. So, as first solution we tried a MAL reaction using photons just as a reactant more:

$$v = k * [Photosystem\ antenna] * hv$$

But this equation resulted in a linear increase beyond the concentration constraints of the model, which led to an inability to reach the equilibrium. Finally, as a compromise, we opted to use a standard Michaelis-Menten equation using the antenna concentration as substrate, until we get a more effective model of light.

- **Reverse reaction of excited antennas**

Both activated P680 and P700 can spontaneously dissipate the energy provided by the light and return to a neutral state without giving the electron to the next acceptor (Yerkes et al, 1983; Evans et al., 1975). The presence of this reverse reaction is induced by several components (e.g temperature). However, we opted here to model these reactions as simple MAL equations:

$v = k * [Photosystem\ antenna]$

This way, we can easily control the rate of the reaction, since changing only the k value we can control the percentage of P680a/P700a that returns to the neutral state.

- **Cytochrome b6f and the PQ cycle**

The cytochrome b6f is the most complex element in this model, because of the PQ cycle. First iterations included both the semiplastoquinone and reactions taking place in $heme_{bp}$ and $heme_{bn}$ modeled with the ER-HMM equation. However, the fact that the midpoint redox potential of the PQ/PQH2 pair is higher than the midpoint potentials of $heme_{bp}$ and $heme_{bn}$ (Em PQ/PQH2= 80mV vs. Em $heme_{bp}$ =-150), made impossible to use this equation for modelling this cycle.

Also the presence of the SPQ led to a curious situation in which every electron entering in the PQ cycle would duplicate itself, giving two electrons as oputput and thermodynamically breaking the validness of the model.

The final solution was to assume a 100% active PQ cycle, so we can set the reduction rate of $heme_{bp}$ at the same value the reduction of ISP is, and calculate this rate using the ER-HMM which in this case works because the difference between midpoint redox potentials of PQH2 and ISP is positive (Em PQH2= 82mV vs. Em ISP= 290mV):

$$ISP\ reduction\ rate = heme_{bp}\ reduction\ rate \quad \text{(Equation 9)}$$

$$ISP\ reduction\ rate = \frac{v_{max_{PQH2\_ISP}} \frac{PQH2}{K_{PQH2}} \frac{ISP_{ox}}{K_{ISP_{ox}}} - \frac{1}{K_E} \frac{ISP_r}{K_{ISP_r}} \frac{PQ}{K_{PQ}}}{\left(1+\frac{PQH2}{K_{PQH2}}+\frac{PQ}{K_{PQ}}\right)*\left(1+\frac{ISP_{ox}}{K_{ISP_{ox}}}+\frac{ISP_r}{K_{ISP_r}}\right)} \quad \text{(Equation 10)}$$

The electron transmission via the low potential chain was modellized using the E-MM equation, which does not use midpoint redox potential.

For the problem of the SPQ, we decided to get rid of it, and thus shortening the PQ cycle to a shorter, simpler form: instead of PQ receiving an electron from $heme_{bn}$ and forming SPQ, which would come another time to $heme_{bn}$ get reduced to PQH2,

$$heme_{bn_r} + PQ \rightarrow heme_{bn_{ox}} + SPQ$$

$$heme_{bn_r} + SPQ \rightarrow heme_{bn_{ox}} + PQH2$$

We stablished a reaction in which two $heme_{bn}$ would reduce PQ directly to PQH2

$$2\ heme_{bn_r} + PQ \rightarrow 2\ heme_{bn_{ox}} + PQH2$$

This way, the same electrons that enter the cycle leave it, keeping the desired robustness.

- **Carbon, nitrogen and oxygen output**

For energy outputs of the system in the form of carbon fixation and nitrate assimilation, and oxygen reduction, we stablished several reactions. For carbon fixation, an only reaction of CO2 fixation and gliceraldehyde-3-phosphate (G3P) was included:

$$3\ CO2 + 6\ NADPH + 5\ H2O + 9\ ATP \rightarrow G3P + 2\ H\_c + 6\ NADP + 9\ ADP + 8\ PI$$

This reaction was modeled using a E-MM equation, with NADPH and ATP as substrates. Also a reaction to prevent accumulation of G3P was added (G3P->G3P_ext).

Nitrate assimilation using ATP was modelled using the reactions with the following stoichiometry:

$$NO3_{ext} + ATP + H2O \rightarrow NO3 + ADP + Pi$$

$$NO2_{ext} + ATP + H2O \rightarrow NO2 + ADP + Pi$$

Both reactions were modeled using a MAL equation, with ATP as only substrate.

For nitrite reduction into ammonia using ferredoxin, we introduced three reactions with the following stoichiometry:

$$NO3 + 2\ Fd_r + 2\ H_s \rightarrow NO2 + 2\ Fd_{ox} + H2O$$

$$NO2 + 6\ Fd_r + 7\ H_s \rightarrow NH3 + 6\ Fd_{ox} + 2\ H2O$$

Both reactions were modelled using a E-MM equation. Like G3P, a reaction to prevent NH3 accumulation was added (NH3->NH3_ext).

For oxygen reduction, we decided to go without adding Flv 1-3, cytochrome c and cytochrome bd as elements of the model. So as, the oxygen reduction was modelled with reactions with the following stoichiometry:

$$Fd_r + O_2 + 8\,H_c \rightarrow (Flv\,1-3)4\,Fd_{ox} + 2\,H2O$$

$$4\,PC_r + O_2 + 8\,H_s \rightarrow (Cytochrome\ c) \rightarrow 4\,PC_{ox} + 2\,H2O + 4\,H_l$$

$$2\,PQH2 + O_2 \rightarrow (Cytochrome\ bd) \rightarrow 2\,PQ + 2\,H2O$$

All these reactions were modelled using E-MM equations.

- **Ion fluxes and electrochemical potential**

The ion fluxes were modelled using taking only in account passive diffusion across the membrane, though there are not known active pumps for ions in Synechocystis thylakoid´s membrane (only a potassium channel, SynK (Zannetti et al., 2010), which has not been modelled here). The equation used to compute the ion transfer rate is the solution proposed by Zhu for the Nernst-Planck equation in e-photosynthesis.

$$J = P\frac{zF\Delta\Psi\left([I_l]-[I_c]e^{-\frac{zF\Delta\Psi}{RT}}\right)}{1-e^{-\frac{zF\Delta\Psi}{RT}}} \qquad \text{(Equation 11)}$$

Where z is the charge of the ion, F is the Faraday constant, ΔΨ is the electrochemical potential gradient, $[I_l]$ and $[I_c]$ are the concentration of the ion in the lumen and cytoplasm, and P is the permeability for the membrane for each ion.

The electrochemical potential was computed using the equations described before in this same report:

$$\Delta\Psi = \frac{Total\ Charge_{\ lumen} - Total\ Charge_{\ citoplasm}}{Membrane\ capacitance}$$

$$Total\ Charge = F * (2[Ca^{2+}] + 2[Mg^{2+}] + [K^+] + [Cl^-] + [H^+] + [OH^-])$$

- **pH gradient and ATP synthesis**

What makes our model different from other models proposed for the photosynthesis in Synechocystis is that we actively monitor the concentration of protons both in lumen and cytoplasm, instead of giving fixed values. Thus, this model is able to provide dynamic values of pH and pH gradient across the membrane. The pH gradient is computed as a difference between the pH on the lumen and thylakoid:

$$\Delta pH = pH_c - pH_l \qquad \text{(Equation 12)}$$

$$pH_{l/c} = -\log(H_{l/c}) \qquad \text{(Equation 13)}$$

The concentration of the protons in each compartment is provided by the sum of the reaction rates of each reaction involving displacement of protons across the thylakoid membrane.

For the ATP synthesis, we used the equation proposed by Zhu (Zhu et al., 2012), which takes in account both pH gradient and electrochemical gradient:

$$vATP = \frac{vATP_{max}\left([ADP][Pi] - \frac{[ATP]}{kE}\right)}{(K_{mADP}K_{mPi})\left(1 + \frac{[ADP]}{K_{mADP}} + \frac{[Pi]}{K_{mPi}} + \frac{[ATP]}{K_{mAtP}} + \frac{[ADP][Pi]}{K_{mADP}K_{mPi}}\right)} \quad \text{(Equation 14)}$$

$$kE = e^{\left(-\frac{\Delta G}{RT}\right)} \quad \text{(Equation 15)}$$

$$\Delta G = \Delta G° + 0.592 HPR ln\left(\frac{[H_l]}{[H_s]}\right) + HPR\Delta\Psi \quad \text{(Equation 16)}$$

Where the K_m`s are the Michaelis-Menten constants for ADP, Pi and ATP; ΔG° is the standard Gibbs free energy for this reaction; HPR is the proton to ATP ratio, which in this case is 4.67 (Vollmar et al., 2009), H_l and H_s are the concentration of protons in lumen and cytoplasm, and ΔΨ is the electrochemical gradient.

- **Hydrogen synthesis**

The synthesis of hydrogen was modelled using a Michaelis-Menten competitive inhibited kinetic. We set both NADPH and ferredoxin as electron donors to protons, with the following stoichiometry:

$$2\ Fd_r + 2\ H_c \rightarrow (Ni - Fe\ hydrogenase) \rightarrow 2\ Fd_{ox} + H_2$$

$$NADPH + 2\ H_c \rightarrow (Ni - Fe\ hydrogenase) \rightarrow NADP + H_2$$

The equations used in the model have the next form:

$$vNADPH\_H2 = \frac{v_{\max\_vNADPH\_H2}[NADPH]}{K_{NADPH\_}\left(1 + \frac{O_2}{kI_{O_2}}\right) + [NADPH]} \quad \text{(Equation 17)}$$

$$vFd\_H2 = \frac{v_{\max\_vFd\_H2}[Fdr]}{K_{Fd}\left(1 + \frac{O_2}{kI_{O_2}}\right) + [Fdr]} \quad \text{(Equation 18)}$$

where kI_{02} is the inhibition constant for oxygen.

4.3 Testing the model: robustness and possibilities

As said previously, one of the main goals of the model is it to be thermodynamically robust; this mean, the electron input is the same as the electron output. The robustness of the model was probed with two tests. The first one consists of measuring the amount of electrons present in the ETC treating the electrons as one molecule more; for that, a differential equation including the sum of all input (Water Splitting) and output (C and N assimilation, oxygen reduction and hydrogen synthesis) rates was created. The second one, a derivation of the first one, consists of measure the sum of these inputs and output rates each unit of time (Fig. 20).

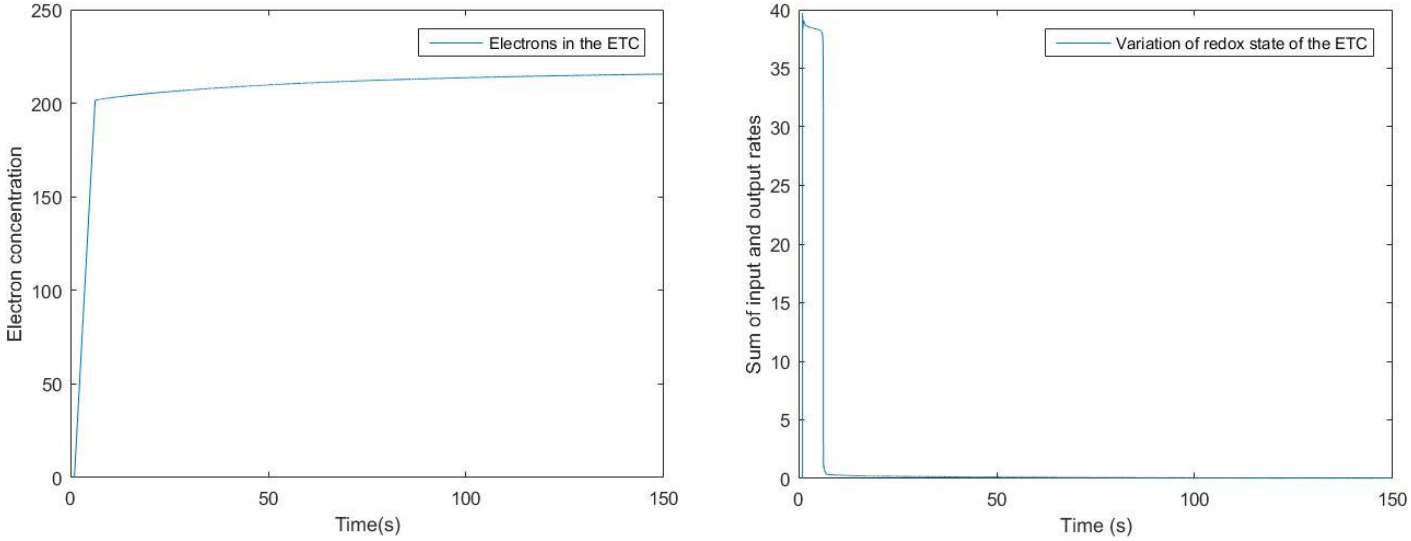

***Figure 20**. Electron concentration in the ETC (left) and sum of the reaction rates of all input and outputs of the model (right).*

As we see, there is an acute filling of the ETC in the early stages, followed by a stabilization of the redox state of the chain. The sum of input and output reactions confirms us the robustness of the model, since it demonstrates that the model quickly stabilizes, making the energy inputs the same as the energy outputs.

While the model is still in a very early stage of development and no work about biological kinetic constants and quantities in the real world has been introduced to the date, this doesn´t means that no significant experiments about several dynamics can be done with it. Two of the tests made with the model are the measurement of the PQ Pool redox state and the production of hydrogen by shutting down other electron skinks:

PQ Pool redox state

Three possibilities were tested here: the first one, a normal state in which both oxidation of PQH2 by cytochrome b6f and cytochrome bd are active (Fig. 21):

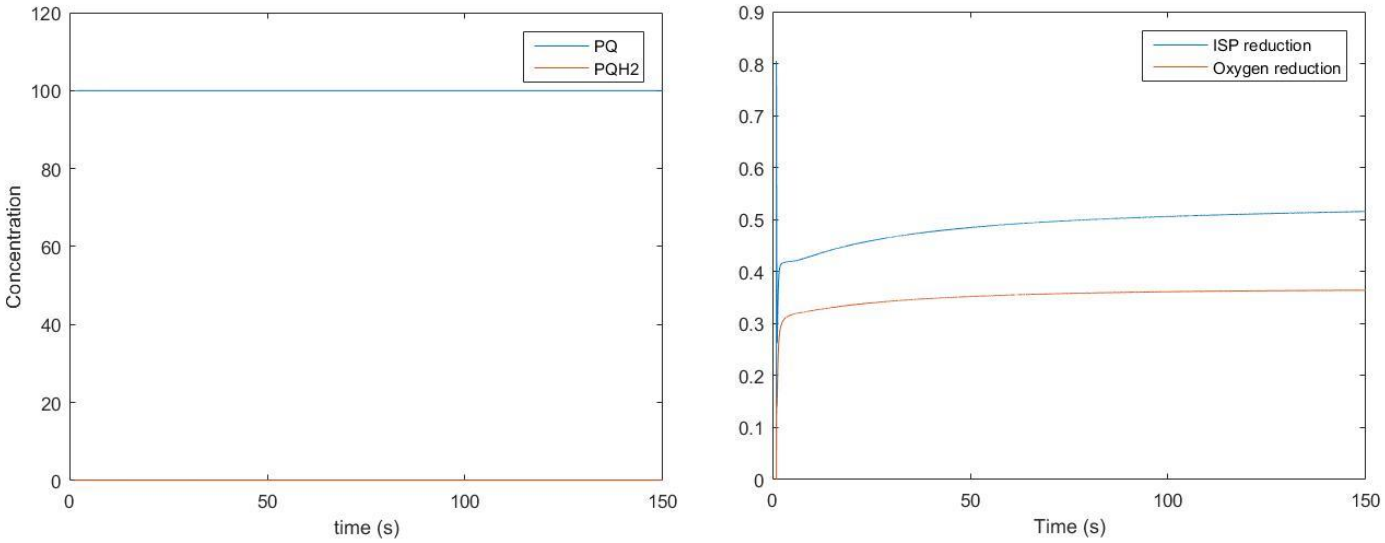

***Figure 21**. Redox state of the PQ pool (left) and oxidation rate of PQH2 (right) under normal conditions*

As we see, almost all the PQ is in the oxidized form. The reaction rate on the ISP is higher than the one in cytochrome bd, since the cytochrome bd develops a high activity when there PQ Pool is greatly reduced . The next test consists of shutting down the cytochrome b6f (equivalent to a gene knock-out) (Fig. 22):

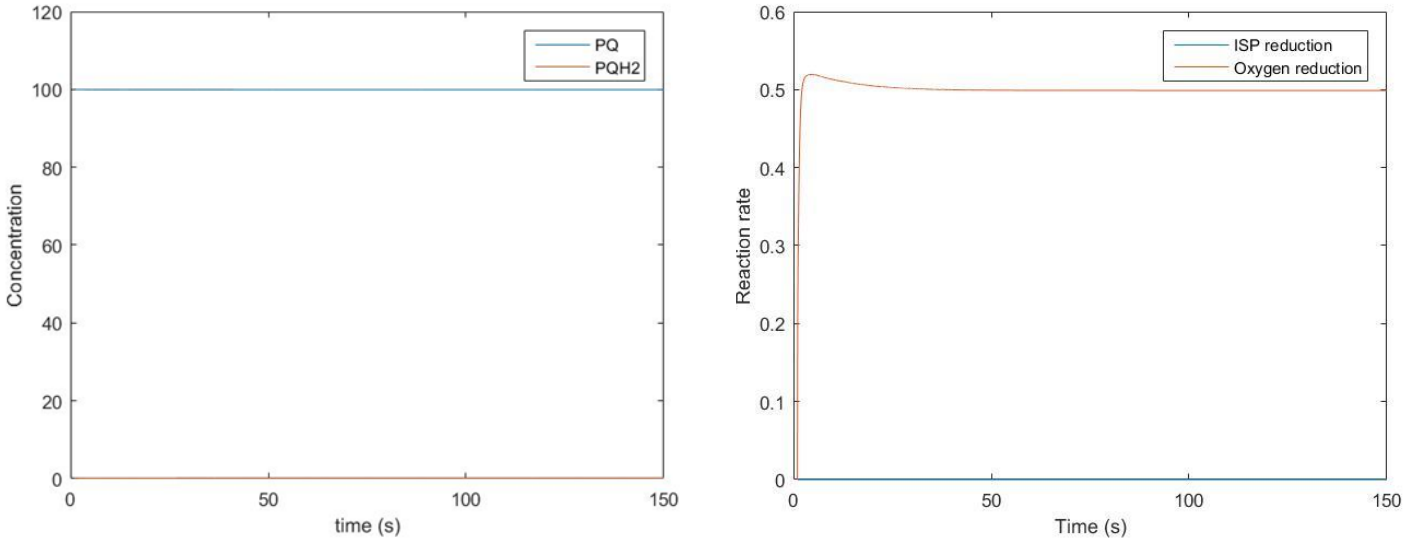

***Figure 22**. Redox state of the PQ pool (left) and oxidation rate of PQH2 (right) without active cyt b6f*

In this case, the redox state of the PQ pool is the same, since the cytochrome bd redirects the electrons that are not entering the cytochrome b6f. The last test consists of shutting

own both cytochrome b6f and cytochrome bd. In this case, the redox state of the pool suffers significant variations (Fig. 23):

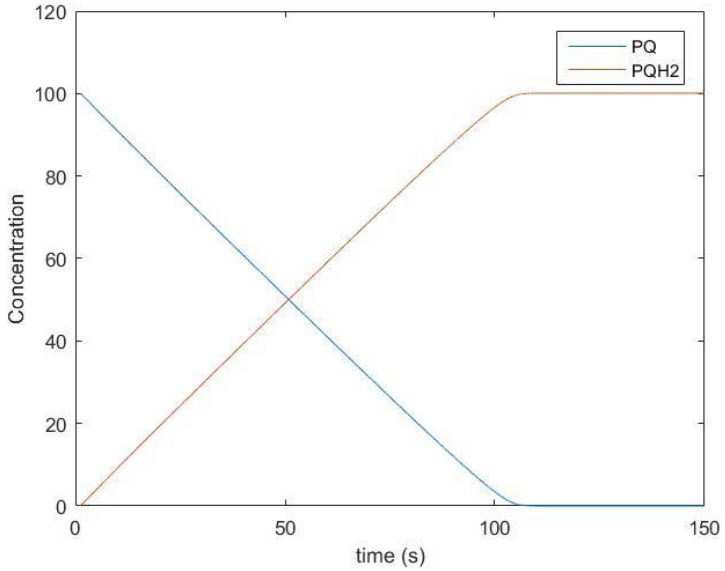

***Figure 23**. Redox state of PQ pool when cyt b6f and cyt bd are inactivated*

We can observe an over reduction of the PQ pool: since there are no electron acceptors the PQH2 can give electrons to, the PQ pool slowly gets reduced to the point there is no PQ available.

Hydrogen synthesis.

The main goal of the project is to develop a tool that can allow metabolic engineers to enhance the hydrogen production in Synechocystis sp. PCC 6803. As discussed previously in this review, the way to get that is to redirect the flow of electrons into the Ni-Fe hydrogenase as much as possible. The model can allow us to simulate what could happen in this situation. First, the production of hydrogen with presence of oxygen and all the output routes opened (Fig. 24):

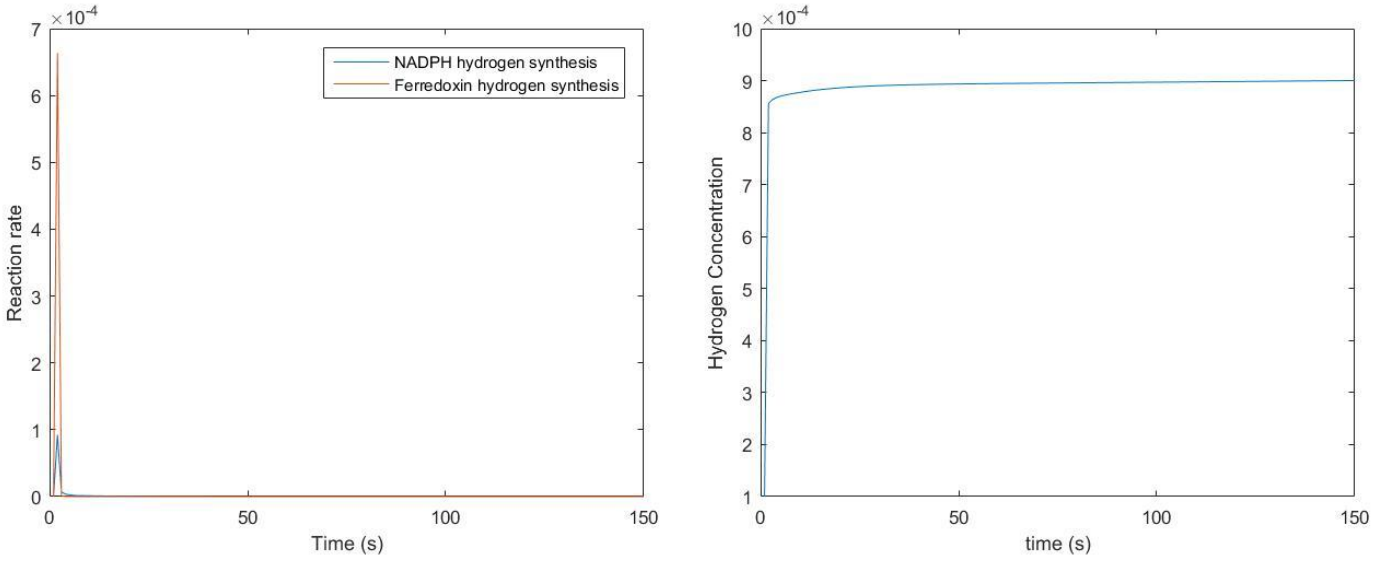

***Figure 24**. Hydrogen production with nitrate assimilation and carbon fixation, and presence of oxygen*

As we see, both the production of hydrogen and the hydrogenase activity are insignificant. Now, using this model we can test a scenario in which there is only oxygen as electron sink (Fig. 25):

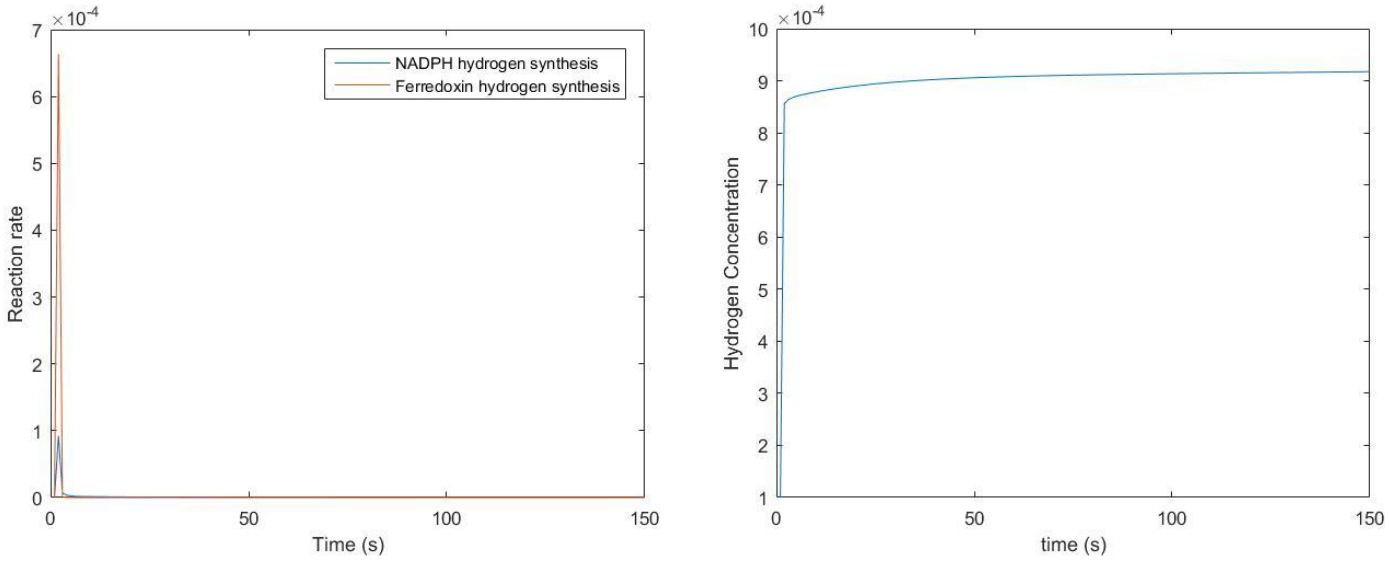

***Figure 25**. Hydrogen production without nitrate assimilation and carbon fixation, and presence of oxygen.*

The results indicate that the influence of the O2 is still too great for the hydrogenase to synthetize any hydrogen, despite no electrons are going to carbon fixation and nitrate assimilation. The last test will simulate anoxic condition added to a complete absence of carbon and nitrate assimilation (Fig. 26). Although this situation is unreachable in vivo without cellular death, the model can allow us to simulate situations even this extreme:

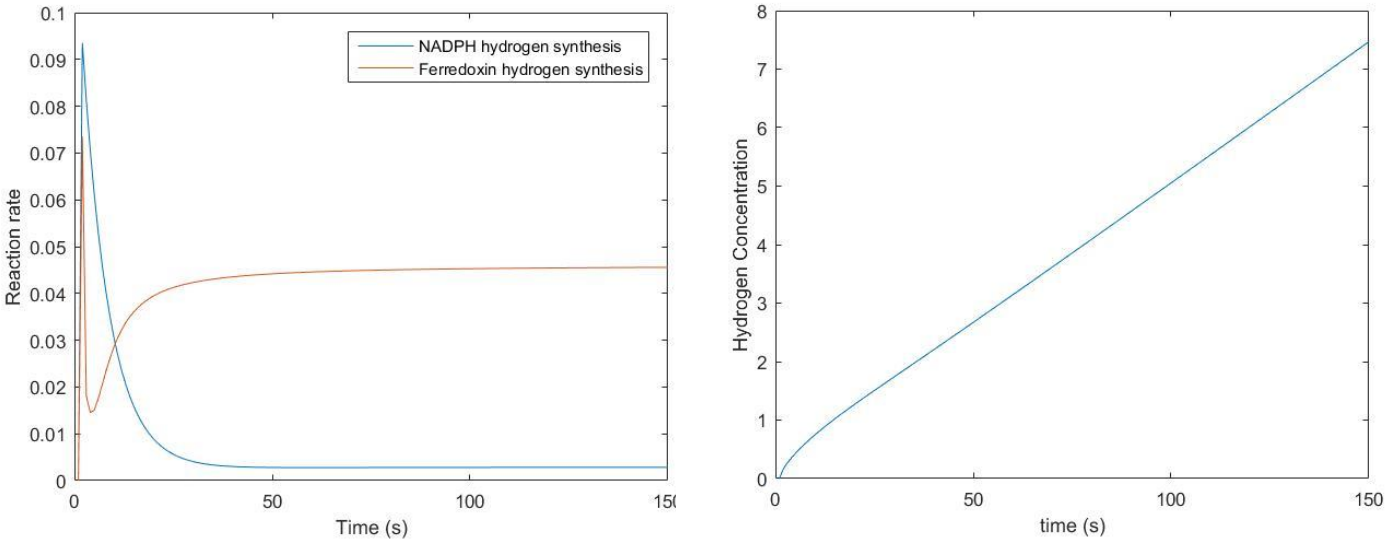

***Figure 26**. Hydrogen production in anoxic conditions without carbon fixation and nitrate assimilation*

This time the results are quite different: there is a small but significant and constant production of hydrogen in the cell, which accumulates over time. Additionally, using different kinetic constants can allow us to simulate a higher production of hydrogen by the ferredoxin as electron donor, as it happens in the real world.

Although these results have no biological relevance, it is good to see how the model reacts to simple modifications of the ETC and provide patterns that can be used by metabolic engineers to drive their experiments and enhance their results. With further development and high-throughput data added to the model, the possibilities are infinite.

4.4 Next steps in the development of the model

Despite many reactions and processes have been pictured into this model, there are still many other mechanisms that we analyzed but finally didn´t make into the latest version of the model:

- **Orange Carotenoid Protein**

The Orange Carotenoid Protein (OCP) is a photoactive protein responsible of the non-photochemical quenching photoprotective (NPQ) mechanism taking place in the Photosystem II in Synechocystis (Kirilovski and Kerfeld, 2011). This OCP is exclusive of cyanobacteria; in higher organisms, the NPQ is mediated by the LhcII antenna, which under low pH conditions switches from a very efficient collector of energy to a very efficient energy dissipator.

When an excess of light falls upon the PSII, the OCP suffers a conformational change and switches to a red form, which associates with the phicobilisomes and lead to an increase of the energy dissipation in the form of heat, and therefore decreasing the amount of energy arriving at the reaction centers.

- **pH influence in the ETC rates**

pH variation have strong influence in various reactions across the ETC; extremely low luminal pH can lead to the interruption of these reactions. There is at least four known reactions in the ETC that are known to be very influenced by pH:

  - Water splitting at OEC (Schiller and Dau, 2000).
  - Quinol reduction at Q_A site (Taly et al., 2003).
  - ISP reduction by plastoquinol (Hong et al., 1999).

- **Respiratory chain and Calvin Cycle**

Despite the photosynthetic apparatus is the main energy source for photobiological hydrogen production in Synechocystis, the respiratory chain also has a strong bearing in the behavior of the ETC. This respiratory chain is tightly connected to the Calvin Cycle , so properly modelling this relation can empower even more the results given by the model.

Our goal is to introduce these features in next versions of the model, thus creating a more powerful tool for metabolic engineers.

5. Conclusions

Since the rise of the Industrial Revolution, mankind has developed a strong dependence on fossil fuels. This situation has led to numerous economical, geopolitical and environmental problems, which makes the necessity of finding an alternative a mandatory issue. Amongst all the proposals, hydrogen stands out as one of the cleanest, cheapest and safest.

There exists many ways to produce hydrogen using renewable energy, but the one with most potential is the photobiological hydrogen production pathway. This technique is based on the potential of the oxygen-intolerant [Ni-Fe] reversible hydrogenase coupled to the photosynthetic electron transport chain of these organisms. The challenges for metabolic engineers to improve the production of biohydrogen reside on redirecting most of the electron flow of the photosynthetic electron transport chain into this hydrogenase, while trying to improve its-oxygen tolerance.

Using an approach based on Systems Biology, a computational model of the photosynthetic electron transport chain of Synechocystis sp. PCC 6803 was created using MATLAB as numerical computing environment. This model gathers 37 different reactions carried out by 45 different protein complexes, electron carriers and enzymes; from water splitting in the Oxygen Evolving Complex of the Photosystem II to nitrate assimilation, including the [Ni-Fe] oxygen-intolerant reversible hydrogenase.

Although this model is still in a very early stage of development, it provides enough functionality to simulate interesting tendencies, such as hydrogen production under several different conditions. With further evolution and the addition of high-throughput data, next iterations of the model will be able to provide researchers with more precise simulations, becoming a powerful tool to support their experiments and investigations.

While still in its infancy, the computational Systems Biology suppose the next revolution on the development of new biotechnological solutions based on metabolic and genetic engineering, since the in silico simulations approach can allow researchers saving huge economic and time costs. As biotechnologists, is our duty to push the possibilities of this discipline to its own very limits; with enough dedication, the possibilities will become virtually infinite.

6. Literature

1. ALLAHVERDIYEBA Y. (2013). Flavodiiron proteins FLV1 and FLV3 enable cyanobacterial growth and photosynthesis under fluctuating light. *PNAS*, 110(10):4111-4116.
2. ANN RAN F. (2013). Genome engineering using the CRISPR-Cas9 system. *Nat Protoc.*, 8(11): 2281-2308.
3. ANTAL T. (2013). Photosynthesis related equations for education and modelling. *Photosynth Res*., 117:1-30.
4. BANIULIS D. (2008). Structure-Function of the cytochrome b_6f Complex. *Photochemistry and Photobiology*, 84:1349-1358.
5. BARTH P. (1998). Ferredoxin reduction by Photosystem I from Synechocystis sp. PCC 6803: toward an understanding of the respective roles of subunits PsaD and PsaE in ferredoxin binding. *Biochemistry*, 37:16233-16241.
6. BP p.l.c. (2015), BP Statistical Review of World Energy June2016.
7. BRETTEL K. (1997). Electron transfer and arrangement of the redox cofactors in photosystem I. *Biochimica et Biophysica Acta*, 1318:322-373.
8. CANO M. (2014). Improved oxygen tolerance for the Synechocystis sp. PCC 6803 bidirectional hydrogenase by site-directed mutagenesis of putative residues of the gas diffusion channel. Int. Journal of Hydrogen Energy, 39: 16872-16884
9. CAPE J (2007). A semiquinone intermediate generated at the Qo site of the cytochrome bc1 complex: Importance for the Q-cycle and superoxide production. *Proc. Natl Acad. Sci. USA*, 104:7887‑7892.
10. CARDONA T. (2011). Charge separation in Photosystem II: A comparative and evolutionary overview. *Biochimica et Biophysica Acta*, 1817:26-43.
11. CHECCHETTO V. (2013). Regulation of photosynthesis by ion channels in cyanobacteria and higher plants. Biophysical Chemistry, 182:51-57.
12. DEXTER J (2009). Metabolic engineering of cyanobacteria for ethanol production. *Energ. Environ Sci.,* 2:857–864.
13. EVANS MCW. (1975). Primary electron acceptor complex of photosystem I in spinach chloroplasts. *Nature*, 256:668-670.
14. FARGIONE J. (2008). Land Clearing and the Biofuel Carbon Debt. *Science*, 94:1235
15. FCH JU (2015). Study on Hydrogen from Renewable Resources in the UE. FCH JU, Brussels, Belgium.
16. FERREIRA KN. (2004). Architecture of the Photosynthetic Oxygen-Evolving Center. *Science*, 303:1831.
17. GRIGORIEVA G. (1982) Transformation in the cyanobacterium Synechocystis sp. 6803. *FEMS Microbiol. Lett.,* 13:367–370.
18. GROTJOHANN I. (2005). Structure of cyanobacterial Photosystem I. *Photosynthesis Research*, 85:51-72.
19. GUTEKUNST K. (2014). The Bidirectional NiFe-hydrogenase in Synechocystis sp. PCC 6803 Is Reduced by Flavodoxin and Ferredoxin and Is Essential under Mixotrophic, Nitrate-limiting Conditions. *Journal of Biological Chemistry*, 289(4):1930-1937.

20. GUTTHANN F. Inhibition of respiration and nitrate assimilation enhances photohydrogen evolution under low oxygen concentrations in *Synechocystis* sp. PCC 6803. *Biochimica et Biophysica Acta*, 1767:161-169.
21. HALL DO. (1995).The potential applications of cyanobacterial photosynthesis for clean technologies. *Photosynthesis research,* 46:159-167.
22. HASTINGS G. (1994). Observation of the reduction and reoxidation of the primary electron acceptor in photosystem I. *Biochemistry*, 33:3913-3200.
23. HEISKE M. (2014). Modelling the respiratory chain complexes with biothermokinetic equations – The case of complex I. *Biochimica er Biophysica Acta*, 1837:1707-1716.
24. HELLINGWERF KJ. (2009). Alternative routes to biofuels: light-driven biofuel formation from CO2 and water based on the "photanol" approach. *J Biotechnol.,* 142:87–90.
25. HEMMERICH P. (1977). Flavin and 5-deazaflavin: a chemical evaluation of 'modified' flavoproteins with respect to the mechanisms of redox biocatalysis. *FEBS Lett.,* 84(1):5–21.
26. HERVÁS M. (1993). *Synechocystis* sp. PCC 6803 plastocyanin isolated from both the cyanobacterium and E.coli transformed cells are identical. *FEBS Letters,* 319(3):257-260.
27. HONG S. (1999). The Energy Landscape for Ubihydroquinone Oxidation at the Q_o site of the bc_1 complex in *Rhodobacter sphaeroides*. *Journal of Biological Chemistry*, 274(48):33931-33944.
28. HOWITT CA. (1998). Quinol and Cytochrome Oxidases in the Cyanobacterium *Synechocystis* sp. PCC 6803. Biochemistry, 37:17944-17951.
29. IKEUCHI M. (2001). *Synechocystis* sp. PCC 6803 – a useful tool in the study of the genetics in cyanobacteria. *Photosynthesis Research*, 70:73-83.
30. IMASHIZUMU M. (2011). Regulation of F_0F_1-ATPase from Synechocystis sp. PCC 6803 by γ and ε subunits is significant for Light/Dark adaptation. *Journal of Biological Chemistry*, 286(30):26595-26602.
31. IPCC(2014): Climate Change 2014: Synthesis Report. Contribution of Working Groups I, II and III to the Fifth Assessment Report of the Intergovernmental Panel on Climate Change [Core Writing Team, R.K. Pachauri and L.A. Meyer (eds.)]. IPCC, Geneva, Switzerland, 151 pp.
32. KANEKO T. (1996) Sequence analysis of the genome of the unicellular cyanobacterium Synechocystis sp. strain PCC 6803. II. Sequence determination of the entire genome and assignment of potential protein-coding regions. *DNA Res*, 3:109–136.
33. KARPLUS PA. (1991). Atomic Structure of Ferredoxin-$NADP^+$ Reductase: Prototype for a Structurally Novel Flavoenzyme Family. *Science*, 251:60-62.
34. KE B. (2001). The Iron–Sulfur Center FeS-X of Photosystem I, The Photosystem-L Core Complex, and Interaction of the FeS-X Domain with FeS-A/FeS-B. *Photosynthesis*, Springer, Netherlands, 527–554.
35. KEASLING J. (2010). Manufacturing Molecules through Metabolic Engineering. *Science*, 330:1355.
36. KIRILOVSKI D. (2011). The orange carotenoid protein in photoprotection of photosystem II in cyanobacteria. *Biochimica et Biophysica Acta*, 1817:158-166.
37. KITANO H. (2002a). Systems Biology: A Brief Overview. *Science*, 295:1662.
38. KITANO H. (2002b). Computational Systems Biology. *Nature*, 420:206-210.
39. KOK B. (1970). Cooperation of charges in photosynthetic O2 evolution-I. A linear four step mechanism. *Photochemistry and Photobiology*, 11:457-475.

40. KRAMER DM. (2011). The importance of Energy Balance in Improving Photosynthetic Productivity. *Plant Physiology*, 155:70-78.
41. LOVENBERG W. (1963). Studies on the Chemical Nature of Clostridial Ferredoxin. Journal of Biological Chemistry, 238(12):3899-3913.
42. MCINTOSH C. (2011). The[Ni_Fe] hydrogenase of the Cyanobacterium Synechocystis sp. PCC 6803 works bidirectionally with a Bias to H2 production. *J. Am. Chem. Soc*., 133:11308-11319.
43. MITCHELL P. (1975). The protonmotive Q Cycle: A general formulation. FEBS Letters, 59(2) 137-139.
44. MOGI T. (2009). Properties of Cytochrome bd Plastoquinol Oxidase from the Cyanobacterium *Synechocystis* sp. PCC 6803. *J. Biochem*., 145(3):395-401.
45. MUNEKAGE Y.(2002). PGR5 is involved in Cyclic Electron Flow around Photosystem I and is essential for Photoprotection in Arabidopsis. *Cell*, 110:361-371.
46. Paris Agreement, United Nations Treaty Collection. 8 July 2016.
47. QUINTANA N. (2011). Renewable energy from Cyanobacteria: energy production optimization by metabolic pathway engineering. *Appl. Microbiol. Biotechnol.*, 91:471-490.
48. RIPPKA R. (1979) Genetic assignments, strain histories and properties of pure cultures of cyanobacteria. *J Gen Microbiol.,* 111: 1–61.
49. RITTMANN BE. (2008). Opportunities for renewable bioenergy using microorganisms. *Biotechnol. Bioeng*., 100(2):203–212.
50. SCHILLER H. (2000). Preparation protocols for high-activity Photosystem II membrane particles of green algae and higher plants, pH dependence of oxyen evolution and comparison of the S_2-state multiline signal by X-band EPR spectroscopy. *J. Photochem. Photobio. B: Biol*, 55:138-144.
51. SCHUURMANS R. (2014) The redox potential of the Plastoquinone Pool of the Cyanobacterium Synechocystis Species Strain PCC 6803 is under Strict Homeostatic Control. *Plant Physiology*, 165:463-475.
52. STEPHANOPOULOS G. (1999). Metabolic Fluxes and Metabolic Engineering. Metabolic Engineering, 1:1-11.
53. TALY A. (2003). The position of Q_B in the Photosynthetic Reaction Center Depends on pH: A theoretical Analysis of the Proton Uptake upon Q_B Reduction. Biophysical Journal, 84:2090-2098.
54. VERMAAS W. (2001). Photosynthesis and respiration in cyanobacteria. *Macmillan Publishes Ltd*, New York, NY, U.S.A.
55. VERSHUBSKII AV. (2014). Modelling of the Photosynthetic Electron Transport Regulation in Cyanobacteria. *Membrane and cell Biology*, 8(3):262-278.
56. VOLLMAR M. (2009). Structure of the c14 rotor ring of the proton translocating chloroplast ATP synthase. Journal of Biological Chemistry, 284:18228-18235.
57. WILLIAMS JGK. (1988) Construction of specific mutations in Photosystem II photosynthetic reaction center by genetic engineering methods in Synechocystis 6803. *Methods Enzymol.,* 167: 766–778.
58. YERKES CT. (1983). A Tris-induced change in the midpoint potential of Z, the donor to photosystem II, as determined by the kinetics of the back reaction. FEBS Letters, 158(2):359-363.

59. ZANETTI M. (2010). A novel potassium channel in photosynthetic cyanobacteria. *PloS ONE*, 5(4):e10118.
60. ZHANG P. (2004). Expression and Functional Roles of the Two Distinct NDH-1 Complexes and the Carbon Acquisition Complex NdhD3/NdhF3/CupA/Sll1735 in Synechocystis sp. PCC 6803. *The Plant Cell*, 16:3326-3340.
61. ZHANG Z. (1998). Electron transfer by domain movement in cytochrome bc1. *Nature*, 392:677-684.
62. ZHU X. (2012). E-photosynthesis: a comprehensive dynamic mechanistic model of C3 photosynthesis: from light capture to sucrose synthesis. *Plant Cell Environ.*, 36(9):1711-27.

SUPLEMMENTARY FILE I. COMPONENTS, CONSTANTS AND REACTIONS OF THE MODEL

The following pages include tables with all the components, reactions with their stoichiometry, physical constants and kinetic constants used in the model; and all the rate equations and differential equations employed in the model.

Table 1. Components of the model with the abbreviations used

Name of the component	Abbreviation (Reduced/Oxidized)
Neutral form of P680 (Photosystem II)	P680
Excited form of P680 (Photosystem II)	P680a
Protonated form of P680 (Photosystem II)	P680p
Q_A site of the Photosystem II	QA_r/QA_o
Non-reduced plastoquinol	PQ
Reduced plastoquinol	PQH2
ISP subunit of cytochrome b6f	ISP_r/ISP_o
$Heme_{bp}$ site of cytochrome b6f	hemebp_r/hemebp_o
$Heme_{bn}$ site of cytochrome b6f	hemebn_r/hemebn_o
Cytochrome f	cytf_r/cytf_o
Plastocyanin	PC_r/PC_o
Neutral form of P700 (Photosystem I)	P700
Excited form of P700 (Photosystem I)	P700a
Protonated form of P700 (Photosystem I)	P700p
A0 chlorophyll (Photosystem I)	A0_r/A0_o
Ferredoxin	Fd_r/Fd_o
Nicotinamide adenine dinucleotide phosphate	NADP
Reduced nicotinamide adenine dinucleotide phosphate	NADPH
Adenosine diphosphate	ADP
Inorganic phosphate	Pi
Adenosine triphosphate	ATP
Protons in the cytoplasm	H_c
Protons in the lumen	H_l
Gliceraldehyde-3-phosphate	G3P
Nitrate	NO3
Nitrite	NO2
Ammonia	NH3
Ion calcium	Ca2+
Ion chloride	Cl-
Ion potassium	K+
Ion magnesium	Mg2+
Oxygen	O2
Hydrogen	H2

Table 2. Reactions in the model, including abbreviation, stoichiometry and rate equation type used.

Reaction	Abb.	Stoichiometry	Equation
Water splitting at OEC	vWS	2 H2O+ 4 P680p -> 4 P680 +4 H_l + O2	MM
Excitation of P680	vP680_P680a	4 P680 + 4 photons -> 4 P680a	MM
Reversion of P680a	vP680a_P680	P680a -> P680	MAL
Reduction of QA	VP680a_QA	4 P680a + 4 QA(ox) <-> 4 P680p + 4 QA(r)	ER-HMM
Reduction of PQ	V2QAr_PQH2	2 QA(r) + 2 H_c + PQ< -> 2 QA(ox) + PQH2	ER-HMM
Reduction of ISP	vPQH2_ISP	PQH2 + ISP(o) <-> SPQ +ISP(r) +2 H(l)	ER-HMM
Reduction of hemebp	vSPQ_hemebp	SPQ + hemebp(o) -> PQ + hemebp(r)	-
Reduction of cytochrome f	vISP_cytf	ISP(r) + cytf(o)< -> ISP(o) + cytf(r)	ER-HMM
Reduction of PC	vcytf_PC	cytf(r) + PC(o) <-> PC(r) + cytf(o)	ER-HMM
Reduction of P700p	vPC_P700	PC(r) + P700p <-> PC(o) + P700	ER-HMM
Reduction of hemebn	vhemebbp_hemebn	hemebp(r) + hemebn(o) ->hemebp(r) + hemebn(o)	E-MM
Reduction of PQ (PQ cycle)	vhemebn_PQH2	2 hemebn(r) + PQ -> 2 hemebn(o) + PQH2	E-MM
Excitation of P700	vP700_P700a	P700 + photon -> P700a	MM
Reversion of P700a	vP700a_P700	P700a -> P700	MAL
Reduction of A0	vP700a_A0r	P700a + A0(o) <->	ER-HMM
Reduction of Ferredoxin	vA0r_Fdr	A0(r) + Fd(o) <-> A0(o) + Fd(o)	ER-HMM
Reduction of NADP	vFdr_NADPH	2 Fd(o) + NADP + H+(c) <-> 2 Fd(r) +NADPH	ER-HMM
ATP Synthesis	vADP_ATP	ADP + Pi + 4.67 H+(l) <-> ATP + 4.67 H+(c)	ATPModule
Short Cycle Around PSI (PGR5)	vFdr_PQH2	2 Fd(r) + PQ + 2 H+(s) <->	ER-HMM
Long Cycle Around PSI (NDH-1)	vNADPH_PQH2	NADPH + PQ <-> NADP + PQ	ER-HMM
G3P synthesis (C output)	vCO2_G3P	3 CO2 + 6 NADPH + 5 H20 + 9 ATP -> G3P + 2 H(c) + 6 NADP + 9 ADP + 8 Pi	E-MM
G3P output	vG3P_G3Pext	G3P -> G3Pext	MAL
Nitrate assimilation (N output)	vNO3ext_NO3	NO3ext + ATP + H2O -> NO3 +ADP +Pi	MAL
Nitrite assimilation (N output)	vNO2ext_NO2	NO2ext + ATP +H2O -> NO2 + ADP +Pi	MAL
Nitrate reduction	vNO3_NO2	NO3 + 2 Fd(r) + 2 H(c) -> NO2 + 2 Fd(o) +H2O	E-MM
Nitrite reduction	vNO2_NH3	NO2 + 6 Fd(r) + 7 H(c) -> NH3 + 6 Fd(o) + 2 H2O	E-MM
NH3 output	vNH3_NH3ext	NH3 -> NH3ext	MAL
Mehler reaction (Flv1-3)	vFlv1_3	4 Fd(r) + 4 H+(c) + O2 -> 4 Fd(o) + 2 H2O	E-MM
PC-mediated oxygen reduction (cyt c)	vPC_H2O	4 PC(r) + O2 + 8 H+(c) -> 4 PC(r) + 2 H2O + 4 H	E-MM
PQH2 mediated oxygen reduction (cyt bd)	vPQH2_H2O	2 PQH2 + O2 -> 2 PQ + 2 H2O	E-MM
O2 output	vO2_O2ext	O2 -> O2ext	MAL
Calcium flux across the membrane	vCa2flux	Ca2+(l) -> Ca2+(c)	Nernst-Planck
Chloride flux across the membrane	vClflux	Cl-(l) -> Cl-(c)	Nernst-Planck
Calcium flux across the membrane	vCa2flux	Ca2+(l) -> Ca2+(c)	Nernst-Planck
Potassium flux across the membrane	vKflux	K+(l) -> K+(c)	Nernst-Planck
Magnessium flux across the membrane	vMg2flux	Mg2+(l) -> Mg2+(c)	Nernst-Planck

NADPH-mediated H2 synthesis	vNADPH_H2	NADPH + 2 H+(c) -> NADP + H2	MM
Fd-mediated H2 synthesis	vFd_H2	2 Fd(r) + 2 H()	MM

Table 3. Physical constants used in the model

Constant	Definition	Value	Units
Vc	Volume of cytoplasm	0.75	ml
Vl	Volume of lumen	0.25	ml
F	Faraday constant	9.649·104	C·mol-1
HPR	Proton to ATP ratio	4.67	Dimensionless
ΔG°	ATP synthesis Gibbs standard free energy	28.1	kJ·mol-1
R	Molar gas constant	8.314	J·K-1·mol1
T	Temperature	298	K
C	Membrane capacitance	1	F
P	Membrane permeability	1	cm·s-1

Table 4. Midpoint redox potentials used in the model (Antal and Kovalenko, 2013)

Redox couple	Midpoint redox potential (mV)
P680a/P680p	-705
QA_o/QA_r	-30
PQ/PQH2	82
ISP_o/ISP_r	290
Cytf_o/Cytf_r	350
PC_o/PC_r	370
P700p/P700	440
P700a/P700p	-1300
A0_o/A0_r	-680
Fd_o/Fd_r	-440
NADP/NADPH	-320

Table 5. Initial concentration values of the components of the model. The values of these initial concentrations are set only for testing purposes, and have no biological relevance

Component	Initial Value
P680	0.1
P680a	0.1
P680p	100
QA_r	0.1
QA_o	100
PQ	100
PQH2	0.1
ISP_o	100
ISP_r	0.1

hemebp_o	100
hemebp_r	0.1
cytf_o	100
cytf_r	0.1
PC_o	100
PC_r	0.1
P700	0.1
P700p	100
P700a	0.1
hemebn_o	100
hemebn_r	0.1
A0_o	100
A0_r	0.1
Fd_o	100
Fd_r	0.1
NADP	100
NADPH	1
ADP	100
Pi	100
ATP	0.1
H_c	1*10-7
H_l	1*10-7
G3P	0.01
NO3	0.01
NO2	0.01
NH3	0.01
Ca2+_l	0.01
Ca2+_c	0.01
Cl-_l	0.01
Cl-_c	0.01
K+_l	0.01
K+_c	0.01
Mg2+_l	0.01
Mg2+_c	0.01
O2	0.0001
H2	0.0001

Table 6. Kinetic constants employed in the model. The values of these kinetic constants are set only for test purposes, and have no biological relevance.

Reaction	Kinetic constant	Value
vWS	vmax_ws	10
	kP680p_r1	0.1
vP680_P680a	Vmax_vP680_P680a	10
	kP680_P680a	0.9
vP680a_P680	kP680a_P680	0.1

vP680a_QA	vmax_vP680a_QA	10
	kP680a_r4	0.1
	kQAo_r4	0.1
	kP680p_r4	1
	kQAr_r4	1
v2QAr_PQH2	vmax_v2QAr_PQH2	10
	kQAr_r5	0.1
	kPQ_r5	0.1
	kQAo_r5	10
	kPQH2_r5	10
vPQH2_ISP	vmax_vPQH2_ISP	10
	kPQH2_r6	0.1
	kISPo_r6	0.1
	kPQ_r6	10
	kISPr_r6	10
vISP_cytf	Vmax_vISP_cytf	10
	kISPr_r8	0.1
	Kcytfo_r8	0.1
	kISPo_r8	10
	Kcytfr_r8	10
vcytf_PC	vmax_vcyf_PC	10
	Kcytfr_r9	0.1
	kPCo_r9	0.1
	Kcyfo_r9	10
	kPCr_r9	10
vPC_P700	vmax_vPC_p70	10
	kPCr_r10	0.1
	kP700p_r10	0.1
	kPCo_r10	10
	kP700_r10	10
vhemebp_hemebn	vmax_vhemebp_hemebn	10
	khemebpr_r11	0.1
	khemebno_r11	0.1
vhemebn_PQH2	vmax_vhemebn_PQH2	1
	khemebn_r12	0.1
	kPQ_r12	0.1
vP700_P700a	Vmax_vP700_P700a	10
	kP700_P700a	0.1
vP700a_P700	K_vP700a_P700	0.01
vP700a_A0r	vmax_vP700a_A0r	10
	kP700a_r15	0.1
	kA0_r15	0.1
	kP700p_r15	10
	kA0r_r15	10
vA0r_Fdr	Vmax_vA0r_Fdr	10
	kA0r_r16	0.1
	kFdo_r16	0.1
	kA0o_r16	10
	kFdr_r16	10
vFdr_NADPH	vmax_vFdr_NADPH	10

	kFdr_r17	0.1
	KNADP_r17	0.1
	kFdo_r17	10
	kNADPH_r17	10
vADP_ATP	vmax_vADP_ATP	10
	kADP_r18	0.1
	kPi_r18	0.1
	kATP_r18	0.1
vFdr_PQH2	vmax_vFdr_PQH2	1
	kFdr_r19	10
	kPQ_r19	10
	kFdo_r19	100
	kPQH2_r19	100
vNADPH_PQH2	vmax_vNADPH_PQH2	1
	kNADPH_r20	10
	kPQ_r20	10
	kNADP_r20	100
	kNPQH2_r20	100
vCO2_G3P	vmax_vCO2_G3P	1
	kNADPH_r21	0.1
	kATP_r21	0.1
vG3P_G3Pext	k_vG3p_G3Pext	1
vNO3ext_NO3	k_vNO3ext_NO3	0.1
vNO2ext_NO2	k_vNO2ext_NO2	0.01
vNO3_NO2	vmax_vNO3_NO2	1
	kNO3_r25	0.01
	kFdr_r25	0.1
vNO2_NH3	vmax_vNO2_NH3	1
	kNO2_r26	0.01
	kFdr_r26	0.1
vNH3_NH3ext	k_vNH3_NH3ext	1
vFlv1_3	vmax_vFlv1_3	1
	kFdr_r28	10
	kO2_r28	1
vPC_H2O	vmax_vPC_H2O	1
	kPCr_r29	10
	kO2_r29	1
vPQH2_H20	vmax_vPQH2_H2O	1
	kPQH2_r30	10
	kO2_r30	1
vO2_O2ext	k_vO2_O2ext	0.01
vNADPH_H2	vmax_vNADPH_H210	10
	kNADPH_r36	1000
vFd_H2	vmax_vFd_H2	10
	kFd_r37	10

Supplementary File II. Rate equations and differential equations of the model

The following pages include the rate equations and differential equations as they have been introduced in the model, including specific kinetic constants for every reaction

Rate Equations

$$vWS = \frac{v_{\max\_ws}[P680p]}{K_{P680p\_r1}+[P680p]} \quad (1)$$

$$vP680\_P680a = \frac{v_{\max\_vP680\_P680a}[P680]}{K_{P680\_P680a}+[P680]} \quad (2)$$

$$vP680\_P680a = kP680a\_P680 * [P680a] \quad (3)$$

$$vP680a\_QA = \frac{v_{\max\_vP680a\_QA}\frac{[P680a]}{kP680a\_r4}\frac{[QAo]}{kQAo\_r4} - \frac{1}{K_E}\frac{[P680p]}{kP680p\_r4}\frac{[QAr]}{kQAr\_r4}}{\left(1+\frac{[P680a]}{kP680a\_r4}+\frac{[P680p]}{kP680p\_r4}\right)*\left(1+\frac{[QAo]}{kQAo\_r4}+\frac{[QAr]}{kQAr\_r4}\right)} \quad (4)$$

$$v2QAr\_PQH2 = \frac{v_{\max\_v2QAr\_PQH2}\frac{[QAr]}{kQAr\_r5}\frac{[PQ]}{kPQ\_r5} - \frac{1}{K_E}\frac{[QAo]}{kQAo\_r5}\frac{[PQH2]}{kPQH2\_r5}}{\left(1+\frac{[QAr]}{kQAr\_r5}+\frac{[QAo]}{kQAo\_r5}\right)*\left(1+\frac{[PQ]}{kPQ\_r5}+\frac{[PQH2]}{kPQH2\_r5}\right)} \quad (5)$$

$$vPQH2\_ISP = \frac{v_{\max\_vPQH2\_ISP}\frac{[PQH2]}{kPQH2\_r6}\frac{[ISPo]}{kISPo\_r6} - \frac{1}{K_E}\frac{[PQ]}{kPQ\_r6}\frac{[ISPr]}{kISPr\_r6}}{\left(1+\frac{[PQH2]}{kPQH2\_r6}+\frac{[PQ]}{kPQ\_r6}\right)*\left(1+\frac{[ISPo]}{kISPo\_r6}+\frac{[ISPr]}{kISPr\_r6}\right)} \quad (6)$$

$$vSPQ\_hemebp = vPQH2\_ISP \quad (7)$$

$$vISP\_cytf = \frac{v_{\max\_vISP\_cytf}\frac{[ISPr]}{kISPr\_r8}\frac{[cytfo]}{kcytfo\_r8} - \frac{1}{K_E}\frac{[ISPo]}{kISPo\_r8}\frac{[cytfr]}{kcytfr\_r8}}{\left(1+\frac{[ISPr]}{kISPr\_r8}+\frac{[ISPo]}{kISPo\_r8}\right)*\left(1+\frac{[cytfo]}{kcytfo\_r8}+\frac{[cytfr]}{kcytfr\_r8}\right)} \quad (8)$$

$$vcytf\_PC = \frac{v_{\max\_vcytf\_PC}\frac{[cytfr]}{kcytfr\_r9}\frac{[PCo]}{kPCo\_r9} - \frac{1}{K_E}\frac{[cytfo]}{kcytfo\_r9}\frac{[PCr]}{kPCr\_r9}}{\left(1+\frac{[cytfr]}{kcytfr\_r9}+\frac{[cytfo]}{kcytfo\_r9}\right)*\left(1+\frac{[PCo]}{kPCo\_r9}+\frac{[PCr]}{kPCr\_r9}\right)} \quad (9)$$

$$vPC\_P700 = \frac{v_{\max\_PC\_P700}\frac{[PCr]}{kPCr\_r10}\frac{[P700p]}{kP700p\_r10} - \frac{1}{K_E}\frac{[PCo]}{kPCo\_r10}\frac{[P700]}{kP700\_r10}}{\left(1+\frac{[PCr]}{kPCr\_r10}+\frac{[PCo]}{kPCo\_r10}\right)*\left(1+\frac{[P700p]}{kP700p\_r10}+\frac{[P700]}{kP700\_r10}\right)} \quad (10)$$

$$vhemebp_{hemebn} = \frac{v_{\max\_hembebp\_hemebn}[hemebp_r][hemebn_o]}{\frac{1}{k_{hemebpr_{r11}}k_{hemebno_{r11}}}+\frac{[hemebp_r]}{k_{hemebno_{r11}}}+\frac{[hemebn_o]}{k_{hemebpr_{r11}}}+[hemebp_r][hemebn_o]} \quad (11)$$

$$vhemebn\_PQH2 = \frac{v_{\max\_vhemebn\_PQH2}[hemebn\_r][PQ]}{\frac{1}{k_{hemebnr\_r12}k_{PQ\_r12}}+\frac{[hemebn\_r]}{k_{PQ\_r12}}+\frac{[PQ]}{k_{hemebnr\_r12}}+[hemebn\_r][PQ]} \quad (12)$$

$$vP700\_P700a = \frac{v_{\max\_vP700\_P700a}[P700]}{K_{P680\_P680a}+[P700]} \quad (13)$$

$$vP700a_{P700} = k\_vP700a\_P700 * [P700a] \quad (14)$$

$$vP700a\_A0r = \frac{v_{max\_vP700a\_A0r}\frac{[P700a]}{kP700a\_r15}\frac{[A0o]}{kA0o\_r15}-\frac{1}{K_E}\frac{[P700p]}{kP700p\_r15}\frac{[A0r]}{kA0r\_r15}}{\left(1+\frac{[P700a]}{kP700a\_r15}+\frac{[P680p]}{kP680p\_r4}\right)*\left(1+\frac{[A0o]}{kA0o\_r15}+\frac{[A0r]}{kA0r\_r15}\right)} \quad (15)$$

$$vA0r\_Fdr = \frac{v_{max\_vA0r\_Fdr}\frac{[A0r]}{kA0r\_r16}\frac{[Fdo]}{kFdo\_r16}-\frac{1}{K_E}\frac{[A0o]}{kA0o\_r16}\frac{[Fdr]}{kFdr\_r16}}{\left(1+\frac{[A0r]}{kA0r\_r16}+\frac{[A0o]}{kA0o\_r16}\right)*\left(1+\frac{[Fdo]}{kFdo\_r16}+\frac{[Fdr]}{kFdr\_r16}\right)} \quad (16)$$

$$vFdr\_NADPH = \frac{v_{max\_vFdr\_NADPH}\frac{[Fdr]}{kFdr\_r17}\frac{[NADP]}{kNADP\_r17}-\frac{1}{K_E}\frac{[Fdo]}{kFdo\_r17}\frac{[NADPH]}{kNADPH\_r17}}{\left(1+\frac{[Fdr]}{kFdr\_r17}+\frac{[Fdo]}{kFdo\_r17}\right)*\left(1+\frac{[NADP]}{kNADP\_r17}+\frac{[NADPH]}{kNADPH\_r17}\right)} \quad (17)$$

$$vATP = \frac{vATP_{max}\left([ADP][Pi]-\frac{[ATP]}{kE}\right)}{(K_{mADP}K_{mPi})\left(1+\frac{[ADP]}{K_{mADP}}+\frac{[Pi]}{K_{mPi}}+\frac{[ATP]}{K_{mAtP}}+\frac{[ADP][Pi]}{K_{mADP}K_{mPi}}\right)} \quad (18)$$

$$kE = e^{\left(-\frac{\Delta G}{RT}\right)} \quad (19)$$

$$\Delta G = \Delta G° + 0.592HPRln\left(\frac{[H_l]}{[H_s]}\right) + HPR\Delta\Psi \quad (20)$$

$$vFdr\_PQH2 = \frac{v_{max\_vFdr\_PQH2}\frac{[Fdr]}{kFdr\_r19}\frac{[PQ]}{kPQ\_r19}-\frac{1}{K_E}\frac{[Fdo]}{kFdo\_r19}\frac{[PQH2]}{kPQH2\_r19}}{\left(1+\frac{[Fdr]}{kFdr\_r19}+\frac{[Fdo]}{kFdo\_r19}\right)*\left(1+\frac{[PQ]}{kPQ\_r19}+\frac{[PQH2]}{kPQH2\_r19}\right)} \quad (21)$$

$$vNADPH\_PQH2 = \frac{v_{max\_vNADPH\_PQH2}\frac{[NADPH]}{kNADPH\_r20}\frac{[PQ]}{kPQ\_r20}-\frac{1}{K_E}\frac{[NADP]}{kNADP\_r20}\frac{[PQH2]}{kPQH2\_r20}}{\left(1+\frac{[NADPH]}{kNADPH\_r20}+\frac{[NADP]}{kNADP\_r20}\right)*\left(1+\frac{[PQ]}{kPQ\_r20}+\frac{[PQH2]}{kPQH2\_r20}\right)} \quad (22)$$

$$vCO2\_G3P = \frac{v_{\max\_vCO2\_G3P}[NADPH][ATP]}{\frac{1}{k_{NADPH\_r21}k_{ATP\_r21}}+\frac{[NADPH]}{k_{ATP\_r21}}+\frac{[ATP]}{k_{NADPH\_r21}}+[NADPH][ATP]} \quad (23)$$

$$vG3P\_G3Pext = k\_vG3P\_G3Pext * [G3P] \quad (24)$$

$$vNO3ext\_NO3 = k\_vNO3ext\_NO3 * [ATP] \quad (25)$$

$$vNO2ext\_NO3 = k\_vNO2ext\_NO2 * [ATP] \quad (26)$$

$$vNO3\_NO2 = \frac{v_{\max\_vNO3\_NO2}[NO3][Fdr]}{\frac{1}{k_{NO3\_r25}k_{Fdr\_r25}}+\frac{[NO3]}{k_{Fdr\_r25}}+\frac{[Fdr]}{k_{NO3\_r25}}+[NO3][Fdr]} \quad (27)$$

$$vNO2\_NH3 = \frac{v_{\max\_vNO2\_NH3}[NO2][Fdr]}{\frac{1}{k_{NO2\_r26}k_{Fdr\_r26}}+\frac{[NO2]}{k_{Fdr\_r26}}+\frac{[Fdr]}{k_{NO2\_r26}}+[NO2][Fdr]} \quad (28)$$

$$vNH3\_NH3ext = k\_vNH3\_NH3ext * [NH3] \quad (29)$$

$$vFlv1\_3 = \frac{v_{\max\_vFlv1\_3}[Fdr][O2]}{\frac{1}{k_{Fdr\_r28}k_{O2\_r28}}+\frac{[Fdr]}{k_{O2\_r28}}+\frac{[O2]}{k_{Fdr\_r28}}+[Fdr][O2]} \quad (30)$$

$$vPC\_H20 = \frac{v_{\max\_vPC\_H2O}[PCr][O2]}{\frac{1}{k_{Fdr\_r29}k_{O2\_r29}}+\frac{[PCr]}{k_{O2\_r29}}+\frac{[O2]}{k_{PC\_r29}}+[PCr][O2]} \quad (31)$$

$$vPQH2\_H20 = \frac{v_{\max\_vPQH2\_H2O}[PQH2][O2]}{\frac{1}{k_{PQH2\_r30}k_{O2\_r30}}+\frac{[PQH2]}{k_{O2\_r30}}+\frac{[O2]}{k_{PQH2\_r30}}+[PQH2][O2]} \quad (32)$$

$$vO2\_O2ext = k\_vO2\_O2ext * [O2] \quad (33)$$

$$vNADPH\_H2 = \frac{v_{\max\_vNADPH\_H2}[NADPH]}{K_{NADPH\_r36}\left(1+\frac{O_2}{kI_{O_2}}\right)+[NADPH]} \quad (34)$$

$$vFd\_H2 = \frac{v_{\max\_vFd\_H2}[Fdr]}{K_{Fd\_r37}\left(1+\frac{O_2}{kI_{O_2}}\right)+[Fdr]} \quad (35)$$

$$vCa2flux = P_{Ca2+}\frac{2F\Delta\Psi\left([Ca2+_l]-[Ca2+_c]e^{-\frac{2F\Delta\Psi}{RT}}\right)}{1-e^{-\frac{2F\Delta\Psi}{RT}}} \quad (36)$$

$$vClflux = P_{Cl-}\frac{-F\Delta\Psi\left([Cl-_l]-[Cl-_c]e^{-\frac{-F\Delta\Psi}{RT}}\right)}{1-e^{-\frac{-F\Delta\Psi}{RT}}} \quad (37)$$

$$vKflux = P_{K+}\frac{F\Delta\Psi\left([K+_l]-[K+_c]e^{-\frac{F\Delta\Psi}{RT}}\right)}{1-e^{-\frac{F\Delta\Psi}{RT}}} \quad (38)$$

$$vMg2flux = P_{Mg}\frac{2F\Delta\Psi\left([Mg2+_l]-[Mg2+_c]e^{-\frac{2F\Delta\Psi}{RT}}\right)}{1-e^{-\frac{2F\Delta\Psi}{RT}}} \quad (39)$$

$$NetCharge_l = V_lF(2[Ca2+]_l - [Cl-]_l + [K+]_l + 2[Mg2+]_l) \quad (40)$$

$$NetCharge_c = V_cF(2[Ca2+]_c - [Cl-]_c + [K+]_c + 2[Mg2+]_c) \quad (41)$$

$$\Delta\Psi = \frac{NetCharge_l - NetCharge_c}{C} \quad (42)$$

$$pH_c = -\log([H_c]) \quad (43)$$

$$pH_l = -\log([H_l]) \quad (44)$$

$$\Delta pH = pH_c - pH_l \quad (45)$$

Differential equations

$$dP680 = 4vWS - 4vP680\_P680a + vP680a\_P680 \quad (1)$$

$$dP680a = 4vP680\_P680a - 4vP680\_QA - vP680a\_P680 \quad (2)$$

$$dP680p = -4vWS + 4vP680a\_QA \quad (3)$$

$$dQA_{ox} = -4vP680a\_QA \ + 2v2QAr\_PQH2 \quad (4)$$

$$dQA_r = 4vP680a\_QA - 2v2QAr\_PQH2 \quad (5)$$

$$dPQ = \ -v2QAr\_PQH2 + vPQH2\_ISP \ + 2vPQH2\_H2O - vFdr\_PQH2 - vhemebn\_PQH2 \quad (6)$$

$$dPQH2 = v2QAr\_PQH2 - vPQH2\_ISP + vhemebn\_PQH2 - 2vPQH2\_H20 + vFdr\_PQH2 + vNADPH\_PQH2 \quad (7)$$

$$dISP_{ox} = -vPQH2\_ISP + vISP\_cytf \quad (8)$$

$$dISP_r = vPQH2\_ISP - vISP\_cytf \quad (9)$$

$$dcytf_{ox} = vISP\_cytf - vcytf\_PC \quad (10)$$

$$dcytf_r = -vISP\_cytf + vcytf\_PC \quad (11)$$

$$dPC_{ox} = -vcytf\_PC + vPC\_P700 \quad (12)$$

$$dPC_r = vcytf\_PC - vPC\_P700 \quad (13)$$

$$dP700 = vPC\_P700 - vP700\_P700a + vP700a\_P700 \quad (14)$$

$$dP700p = -vPC\_P700 + vP700a\_A0r \quad (15)$$

$$dP700a = vP700\_P700a - vP700\_A0r - vP700a\_P700 \quad (16)$$

$$dhemebp_{ox} = -vSPQ\_hemebp + vhemebp\_hemebn \quad (17)$$

$$dhemebp_r = vSPQ\_hemebp - vhemebp\_hemebn \quad (18)$$

$$dhemebn_{ox} = -vhemebp\_hemebn + 2vhemebn\_PQH2 \quad (19)$$

$$dhemebn_r = vhemebp\_hemebn - 2vhemebn\_PQH2 \quad (20)$$

$$dA0_{ox} = -vP700\_A0r + vA0r\_Fdr \quad (21)$$

$$dA0_r = vP700\_A0r - vA0r\_Fdr \quad (22)$$

$$dFd_{ox} = -vA0r\_Fdr + 2vFdr\_NADPH + 2vFdr\_PQH2 + 2vNO3\_NO2 + 6vNO2\_NH3 + 4vFlv1\_3 + 2vFd\_H2 \quad (23)$$

$$dFd_{r} = vA0r\_Fdr - 2vFdr\_NADPH - 2vFdr\_PQH2 - 2vNO3\_NO2 - 6vNO2\_NH3 - 4vFlv1\_3 - 2vFd\_H2 \quad (24)$$

$$dNADP = -vFdr\_NADPH + 6vCO2\_G3P + vNADPH\_PQH2 + vNADPH\_H2 \quad (25)$$

$$dNADPH = vFdr\_NADPH - 6vCO2\_G3P - vNADPH\_PQH2 - vNADPH\_H2 \quad (26)$$

$$dADP = -vADP\_ATP + 9vCO2\_G3P + vNO3\_NO3ext + vNO2ext\_NO2 \quad (27)$$

$$dPi = -vADP\_ATP + 9vCO2\_G3P + vNO3\_NO3ext + vNO2ext\_NO2 \quad (28)$$

$$dATP = vADP\_ATP - 9vCO2\_G3P - vNO3\_NO3ext - vNO2ext\_NO2 \quad (29)$$

$$dH_l = \frac{V_c}{V_l}(4vWS + 2vPQH2\_ISP - 4.67vADP\_ATP + 4vPC\_H2O \quad (30)$$

$$dH_c = -2v2QAr\_PQH2 - 2vhemebn\_PQH2 + 4.67vADP\_ATP - 2vNO3\_NO2 - 7vNO2\_NH3 - 4vFlv1\_3 - 8vPC\_H2O - 2vNADPH\_PQH2 \quad (31)$$

$$dG3P = vCO2\_G3P - vG3PG3Pext \quad (32)$$

$$dNO3 = vNO3ext\_NO3 - vNO3\_NO2 \quad (33)$$

$$dNO2 = vNO2ext\_NO2 - vNO2\_NH3 \quad (34)$$

$$dNH3 = vNO2\_NH3 - vNH3\_NH3ext \quad (35)$$

$$dCa2+_l = -vCa2flux\frac{V_c}{V_l} \quad (36)$$

$$dCa2+_c = vCa2flux \quad (37)$$

$$dCl-_l = -vClflux\frac{V_c}{V_l} \quad (38)$$

$$dCl-_c = vClflux \quad (39)$$

$$dK+_l = -vKflux\frac{V_c}{V_l} \quad (40)$$

$$dK+_c = vKflux \quad (41)$$

$$dMg2+_l = -vMg2flux\frac{V_c}{V_l} \quad (42)$$

$$dMg2+_c = -vMg2flux \quad (43)$$

$$dO2 = vWS - vFlv1\_3 - vPC\_H2O - vPQH2\_H2O - vO2\_O2ext \quad (44)$$

$$dH2 = vNADPH\_H2 + vFd\_H2 \quad (45)$$